Prepared for submission to JCAP

arXiv:1111.0292v2 [hep-ph] 29 Feb 2012

Resolving astrophysical uncertainties in dark matter direct detection

Mads T. Frandsen,[a,b] **Felix Kahlhoefer,**[a] **Christopher McCabe,**[a,c] **Subir Sarkar,**[a] **and Kai Schmidt-Hoberg**[a,b]

[a]Rudolf Peierls Centre for Theoretical Physics, University of Oxford, 1 Keble Road, Oxford OX1 3NP, United Kingdom

[b]Theory Division, CERN, 1211 Geneva 23, Switzerland

[c]Institute for Particle Physics Phenomenology, Durham University, South Road, Durham, DH1 3LE, United Kingdom

E-mail: m.frandsen1@physics.ox.ac.uk, felix.kahlhoefer@physics.ox.ac.uk, christopher.mccabe@durham.ac.uk, s.sarkar@physics.ox.ac.uk, ksh@physics.ox.ac.uk

Abstract. We study the impact of the assumed velocity distribution of galactic dark matter particles on the interpretation of results from nuclear recoil detectors. By converting experimental data to variables that make the astrophysical unknowns explicit, different experiments can be compared without implicit assumptions concerning the dark matter halo. We extend this framework to include the annual modulation signal, as well as multiple target elements. Recent results from DAMA, CoGeNT and CRESST-II can be brought into agreement if the velocity distribution is very anisotropic and thus allows a large modulation fraction. However constraints from CDMS and XENON cannot be evaded by appealing to such astrophysical uncertainties alone.

Keywords: Dark matter detectors, Dark matter experiments, Dark matter theory, Galaxy dynamics

Preprint numbers: OUTP-11-52-P, CERN-PH-TH/2011-232, IPPP/11/65, DCPT/11/128

1 Introduction

The direct detection of galactic dark matter (DM) particles in the laboratory using shielded nuclear recoil detectors is among the most challenging and high priority goals of astroparticle physics. Presently several experiments are taking data with the primary aim of securing a convincing detection and thereby confirming the hypothesis that DM is in fact made of relic particles. Several ambitious next-generation experiments are planned and from these we hope to be able to extract the properties of the DM particle, most notably its mass and cross-section for interactions with nucleons. However, there are a number of uncertainties in the interpretation of such experimental data. Foremost among these is our poor knowledge of the distribution and dynamics of DM in our Galaxy. In particular, the DM velocity distribution $f(\boldsymbol{v})$ strongly affects the conclusions we can draw from the data, for example whether the results of different experiments are mutually consistent [1–9].

Results from direct detection experiments are usually presented as a signal or exclusion curve in the parameter plane of DM mass versus its scattering cross-section, *assuming* a Maxwell-Boltzmann (M-B) velocity distribution with a cut-off at the escape velocity from the Galaxy. This is also known as the Standard Halo Model (SHM). There are more sophisticated dynamical models of halo DM but to study the effects of these the plot has to be reproduced separately for all such velocity distributions which can be cumbersome.

One might wonder if the experimental data can itself be used to infer the DM velocity distribution. Unfortunately, this turns out to be rather difficult [10, 11] because a nuclear recoil of energy $E_{\rm R}$ can originate from any DM particle which has a velocity larger than some minimum velocity $v_{\rm min}(E_{\rm R})$. Consequently, rather than probing the velocity distribution, direct detection experiments actually measure the velocity integral: $g(v_{\rm min}) = \int_{v_{\rm min}} f(\boldsymbol{v})/v \, {\rm d}^3 v$.

Hence, it was suggested [12] that results from one experiment be converted into $v_{\rm min}$-space in order to predict the event rate in a second experiment, without having to make any assumptions concerning the astrophysics. While this approach works well in comparing two experiments that are sensitive to a similar range of DM velocities, it is difficult to compare experiments that probe different regions of the velocity distribution. It would therefore be preferable to have a framework in which the astrophysical unknowns are made explicit so one can assess their impact on the extraction of DM properties.

In this paper we investigate in detail the idea, also suggested in Ref.[12], of mapping *all* experimental results into $v_{\rm min}$-space. To do so, we must know the properties of the DM particles — we will assume therefore that their mass can be inferred either from collider experiments or the combined information from several direct detection experiments (see e.g. Ref.[10, 13]). In this sense, our approach is complementary to the usual analysis of direct detection experiments, wherein the astrophysical parameters are held fixed and the DM mass and cross-section are allowed to vary.

Just as the usual presentation of results shows whether all experiments are consistent for some range of DM mass and scattering cross-section, our treatment will illustrate whether it is possible to find a DM velocity distribution that can reconcile all such experimental results. To demonstrate this, we focus on the DM mass range 6–15 GeV motivated by recent claims of signals from DAMA, CoGeNT and CRESST-II [14–16] and show that $g(v_{\rm min})$ can indeed be chosen so as to enable a consistent description of these experiments. However, upper limits on signals from XENON [17] and CDMS [18, 19] *cannot* be evaded by appealing to astrophysical uncertainties alone. If all these experimental results are correct then to resolve the tension between the signals and upper limits requires non-standard DM interactions.

This paper is organised as follows: Section 2 introduces notation and sets out the analysis framework. In Section 3 we discuss how a measurement of the differential event rate in a direct detection experiment can be translated into a measurement of $g(v_{\rm min})$ and how an experiment that does not observe a DM signal can constrain the velocity integral. We present measurements and limits on $g(v_{\rm min})$ for the most relevant direct detection experiments in Section 4 and also assess the compatibility of CoGeNT and CRESST-II. In Section 5 we do a similar analysis for experiments which observe an annual modulation of the event rate and assess the compatibility of DAMA and CRESST-II. In Section 6 we discuss briefly how varying the particle physics properties of DM can affect the analysis, and present our conclusions in Section 7.

2 The velocity integral

The differential event rate in the laboratory frame for the scattering of DM particles on nuclei is given by

$$\frac{{\rm d}R}{{\rm d}E_{\rm R}} = \frac{\rho\,\sigma_n}{2m_\chi\mu_{n\chi}^2}C_{\rm T}^2(A,Z)F^2(E_{\rm R})g(v_{\rm min})\ , \tag{2.1}$$

where ρ is the DM density, m_χ is the DM mass and $\mu_{n\chi}$ is the reduced DM-nucleon mass. The 'velocity integral' $g(v_{\rm min})$ is defined by

$$g(v_{\rm min},t) \equiv \int_{v_{\rm min}}^{\infty}\frac{f(\boldsymbol{v}+\boldsymbol{v}_{\rm E}(t))}{v}\,{\rm d}^3v\ , \tag{2.2}$$

where $f(v)$ is the local DM velocity distribution evaluated in the galactic rest frame, $v=|\boldsymbol{v}|$ and $\boldsymbol{v}_{\rm E}(t)$ is the velocity of the Earth relative to the galactic rest frame [20, 21]. The minimum velocity required for a DM particle to transfer an energy $E_{\rm R}$ to a nucleus is

$$v_{\rm min}(E_{\rm R}) = \sqrt{\frac{m_{\rm N}E_{\rm R}}{2\mu^2}}\ , \tag{2.3}$$

where $m_{\rm N}$ is the mass of the target nucleus and μ the corresponding reduced mass of the DM-nucleus system.

To avoid clutter in our formulae, we define $C_{\rm T}(A,Z)\equiv(f_p/f_nZ+(A-Z))$, where A and Z are the mass and charge numbers of the target nucleus and $f_{n,p}$ denote the effective DM coupling to neutrons and protons, respectively. We assume $f_n/f_p=1$ unless explicitly stated otherwise. Finally, σ_n is the DM-neutron cross-section at zero momentum transfer and $F(E_{\rm R})$ is the nuclear form factor, which encodes the loss of coherence as the momentum transfer deviates from zero. We use the Helm form factor from Ref.[22].

For our purposes, it will be convenient to absorb the DM mass, cross-section and density into the definition of the velocity integral and consider the rescaled velocity integral

$$\tilde{g}(v_{\rm min}) = \frac{\rho\,\sigma_n}{m_\chi}\,g(v_{\rm min})\ , \tag{2.4}$$

which has a typical value in the range $10^{-27}-10^{-22}$ day^{-1} (see Figure 1).

At this point, it is worth developing some intuition for $\tilde{g}(v_{\rm min})$ and elucidating its relation to the more familiar DM velocity distribution $f(v)$. In the left panel of Figure 1, we show the canonical M-B velocity distribution of the SHM, along with a sharply peaked

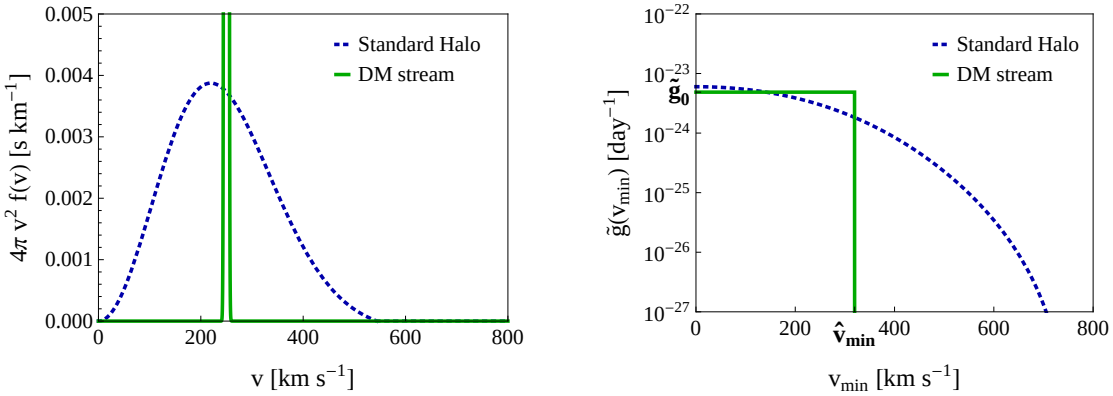


Figure 1. The one-dimensional velocity distribution $4\pi v^2 f(v)$ (left) and the rescaled velocity integral $\tilde{g}(v_{\rm min})$ (right) for the Standard Halo Model (blue, dotted) and a sharply peaked DM stream (green, solid). To calculate $\tilde{g}(v_{\rm min})$, we have assumed $\sigma_n = 10^{-40}$ cm^2, $\rho = 0.3$ GeV/cm^3 and $m_\chi = 15$ GeV. The velocity of the DM stream is $\boldsymbol{v}_{\rm s} = (250,\, 0,\, 0)$ km/s, giving $\hat{v}_{\rm min} = |\boldsymbol{v}_{\rm s} - \boldsymbol{v}_{\rm E}| \approx 330$ km/s.

function which could arise from a stream of DM or alternatively can be thought of as a shifted M-B distribution in the limit of small velocity dispersion. In the right panel we show the corresponding $\tilde{g}(v_{\rm min})$.[1] As observed earlier [23], $\tilde{g}(v_{\rm min})$ has the important property that for *any* velocity distribution it is a decreasing function of $v_{\rm min}$ since $f(v) \geq 0$. As the velocity dispersion decreases, $\tilde{g}(v_{\rm min})$ becomes more like a step-function which is the minimal form consistent with this property.

3 Measurements and constraints

We now discuss how information on $\tilde{g}(v_{\rm min})$ can be extracted from direct detection experiments.[2] First we consider experiments that observe a signal that can be interpreted in terms of DM scattering, namely DAMA, CoGeNT and CRESST-II. In this case, the measured signal can be directly translated into a measurement of $\tilde{g}(v_{\rm min})$. Then there are experiments that do not observe a DM signal above their expected background and thus constrain the differential DM scattering rate which converts into a bound on $\tilde{g}(v_{\rm min})$. Since $\tilde{g}(v_{\rm min})$ may be time-dependent in principle, the resulting limit is strictly speaking on the *average* of $\tilde{g}(v_{\rm min})$ over the period the corresponding experiment was taking data.

3.1 Measuring the velocity integral

It is relatively straightforward to infer the value of $\tilde{g}(v_{\rm min})$ at $v_{\rm min}(E_{\rm R})$ from a nuclear recoil detector such as CoGeNT that consists of a single element and measures the differential event rate $\mathrm{d}R/\mathrm{d}E_{\rm R}$ at the recoil energy $E_{\rm R}$. Inverting Eq. (2.1), we find

$$\tilde{g}(v_{\rm min}) = 2\mu_{n\chi}^2 \, \frac{1}{C_{\rm T}^2(A,Z) F^2(E_{\rm R})} \, \frac{\mathrm{d}R}{\mathrm{d}E_{\rm R}} \,. \tag{3.1}$$

For a real detector we must take the detector resolution ΔE and the detector efficiency $\epsilon(E_{\rm R})$ into account. If the detector measures the differential event rate in the interval $[E_1, E_2]$, we

[1] We neglect the time dependence of $g(v_{\rm min})$ here, which would lead to a slight smearing of the step function.
[2] A similar discussion is presented in the appendix of Ref. [12].

can infer the value of $\tilde{g}(v_{\rm min})$ for $v_{\rm min}$ in the interval $[v_{\rm min}(E_1 - \Delta E), v_{\rm min}(E_2 + \Delta E)]$:

$$\tilde{g}(v_{\rm min}) = 2\mu_{n\chi}^2 \, \frac{1}{C_{\rm T}^2(A,Z) F^2(E_{\rm R}) \epsilon(E_{\rm R})} \, \frac{{\rm d}R}{{\rm d}E_{\rm R}} \, . \tag{3.2}$$

The recoil energy where the nuclear form factor and the efficiency are evaluated should in the range $E_1 < E_{\rm R} < E_2$; we assume that the energy bin is sufficiently small that these quantities do not vary significantly with $E_{\rm R}$ within the bin.[3]

Additional care is required for experiments like DAMA and CRESST-II which have targets with more than one element. The DAMA detector has both sodium and iodine nuclei, the latter being much heavier than the former ($m_{\rm I} \approx 5.5 m_{\rm Na}$). For the light DM we consider, the kinetic energy of the recoiling iodine nucleus is below the energy threshold of the detector so it is a good approximation to assume that all contributions to ${\rm d}R/{\rm d}E_{\rm R}$ come from scattering on Na nuclei and use Eq. (3.2) taking the mass fraction of Na in the detector into account (see Section 5).

For CRESST-II which contains oxygen, calcium and tungsten, the situation is more complicated. Since tungsten is much heavier than oxygen and calcium, we can ignore it as the corresponding recoil energy is below the detector's energy threshold. However oxygen and calcium are relatively close in mass so extracting information on $\tilde{g}(v_{\rm min})$ becomes more complicated. We discuss these difficulties and how to deal with them in Appendix A.

3.2 Constraining the velocity integral

Next we consider experiments that do not measure the differential event rate but are rather able to bound ${\rm d}R/{\rm d}E_{\rm R}$ over some energy range. This is usually converted into a bound on σ_n for a given DM mass, assuming a galactic halo model such as the SHM. Instead we wish to use the bound on ${\rm d}R/{\rm d}E_{\rm R}$ to constrain $\tilde{g}(v_{\rm min})$ for different values of $v_{\rm min}$.[4]

Since $f(v) \geq 0$, the following inequality holds for any value of $v_{\rm min}$:

$$\tilde{g}(v_{\rm min}) \geq \tilde{g}(\hat{v}_{\rm min}) \, \Theta(\hat{v}_{\rm min} - v_{\rm min}) \, , \tag{3.3}$$

where $\tilde{g}(\hat{v}_{\rm min})$ is a constant and $\Theta(x)$ is the Heaviside step function. Of all velocity integrals that have $\tilde{g}(\hat{v}_{\rm min}) = \tilde{g}_0$, the one defined by $\tilde{g}(v_{\rm min}) = \tilde{g}_0 \, \Theta(\hat{v}_{\rm min} - v_{\rm min})$ thus predicts the smallest number of events in any given experiment. Of course $g(v_{\rm min}) \propto \Theta(\hat{v}_{\rm min} - v_{\rm min})$ is not a realistic model for the galactic halo, nevertheless it is a valid velocity integral that can be used to predict the event rate for a given experiment. A more realistic halo must satisfy Eq. (3.3) and will therefore necessarily predict a *larger* event rate. Consequently, if we can reject the case when $\tilde{g}(v_{\rm min}) = \tilde{g}_0 \, \Theta(\hat{v}_{\rm min} - v_{\rm min})$, we can also reject any other other halo model giving $\tilde{g}(\hat{v}_{\rm min}) = \tilde{g}_0$.

Hence if an experiment places an upper bound on ${\rm d}R/{\rm d}E_{\rm R}$, we can correspondingly bound $\tilde{g}(v_{\rm min})$ by fixing $v_{\rm min} = \hat{v}_{\rm min}$ and finding the smallest value of $\tilde{g}(\hat{v}_{\rm min})$ such that the predicted event rate for $\tilde{g}(v_{\rm min}) = \tilde{g}(\hat{v}_{\rm min}) \, \Theta(\hat{v}_{\rm min} - v_{\rm min})$ is *larger* than the measured value (at a given confidence level). Repeating this procedure for all $\hat{v}_{\rm min}$, we obtain a continuous upper bound on $\tilde{g}(\hat{v}_{\rm min})$ — see Figure 2. If the exclusion curve thus obtained touches (or crosses)

[3] This assumption is good for CoGeNT and DAMA for the light DM that we consider. However it is not a good approximation for CRESST-II where $\epsilon(E_{\rm R})$ can change rapidly within a single bin that contains the onset of a new detector module; to avoid this we bin the data so such regions are avoided (see Appendix D).

[4] It is straightforward to put a bound on $\tilde{g}(v_{\rm min})$ from experiments that use a single element; difficulties arising in experiments with more than one type of nuclei are discussed in Appendix A.

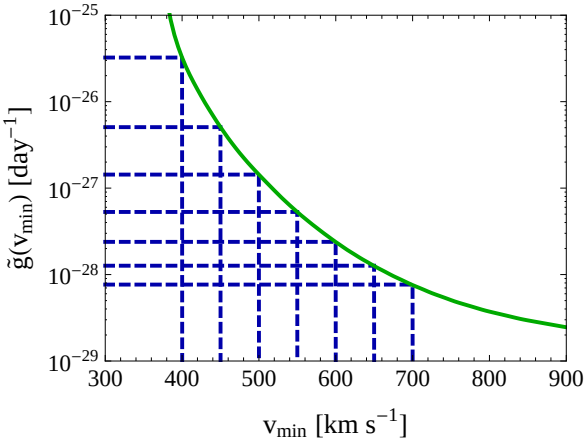


Figure 2. An illustration of the method developed in Section 3.2. The blue dashed lines correspond to velocity integrals of the form $\tilde{g}_0\,\Theta(\hat{v}_{\rm min} - v_{\rm min})$ for different choices of $\tilde{g}_0$ and $\hat{v}_{\rm min}$. The predicted event rate in the XENON100 detector for each of these velocity integrals can be rejected by the data from XENON100. The green line shows the resulting bound on $\tilde{g}(v_{\rm min})$.

the $\tilde{g}(\hat{v}_{\rm min})$ curve for a particular $f(v)$, this model will be excluded by the experimental data at the same confidence level used to construct the exclusion bound. In other words, if the bound on $\tilde{g}(v_{\rm min})$ lies below (some of) the values of $\tilde{g}(v_{\rm min})$ implied by the measured recoil spectrum at DAMA, CoGeNT or CRESST-II, it will not be possible to find a halo model that consistently describes all measurements and evades all experimental bounds.

Note that the converse of this statement is not necessarily true: even if $\tilde{g}(v_{\rm min})$ stays below a given exclusion curve for all values of $v_{\rm min}$, this does not imply that the model is *not* excluded by the corresponding experiment. By construction, we have ensured only that the predicted differential event rate in each individual energy bin is below the respective experimental limit. However, if the measured velocity integral remains close to the exclusion limit over a wide range of $v_{\rm min}$, the predicted total event rate, i.e. the integral of the differential event rate over several bins, may be excluded at the chosen confidence level.

4 Results

Now we use the framework developed in the previous section to analyse recent results from direct detection experiments (discussed in Appendix D). We use the events reported by CoGeNT and CRESST-II to measure $\tilde{g}(v_{\rm min})$ and the null results from XENON, CDMS, SIMPLE and the CRESST-II commissioning run to constrain it. Our results are shown in Figure 3 for various values of the DM mass m_χ. As we increase m_χ the exclusion curves as well as the CoGeNT data points move according to $v_{\rm min} \sim 1/m_\chi$ (which holds when $m_\chi < m_{\rm N}$) — the CRESST-II data points and exclusion curves scale differently because the mass of oxygen is comparable to m_χ in the lower panels. It should be clear from this consideration that the CoGeNT and CRESST-II data points are always excluded for $6\,{\rm GeV} < m_\chi < 15\,{\rm GeV}$.

For all masses considered, one can see the obvious conflict between the measurements by CoGeNT and CRESST-II and the exclusion bounds from other experiments. In each case, most of the measured points lie above one (or more) of the exclusion curves. We conclude that a consistent description of all experiments is not possible for *any* model of the DM

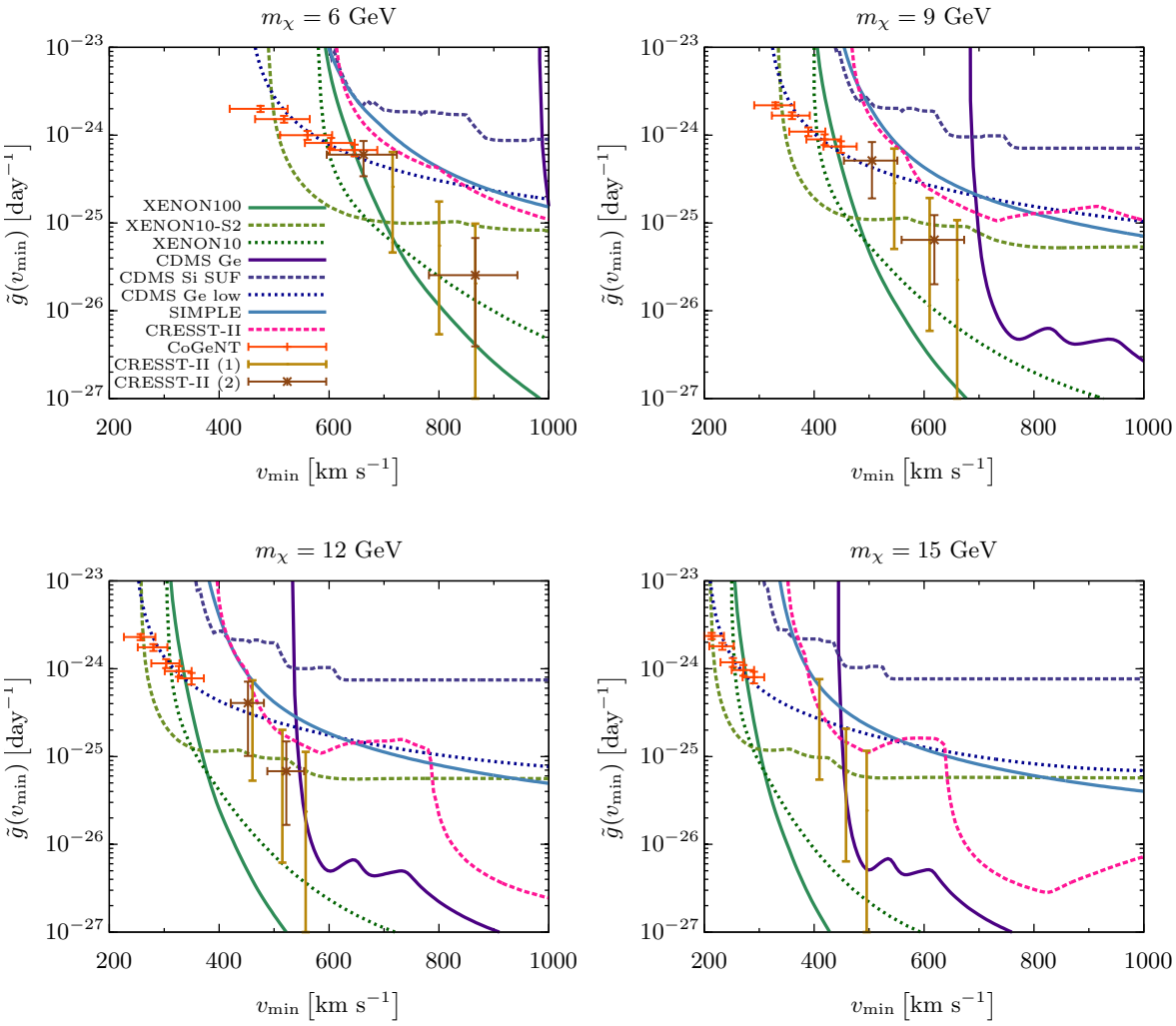


Figure 3. Measurements and exclusion bounds of the velocity integral $\tilde{g}(v_{\rm min})$ for different DM masses m_χ. The DM interaction is spin-independent and elastic with $f_n/f_p = 1$. Values of $\tilde{g}(v_{\rm min})$ above the lines are excluded with at least 90% confidence. For $m_\chi = 6$, 9 and 12 GeV the data points for CRESST-II have been obtained using two different methods, as described in Appendix A. It is not possible to find any model for the DM halo that provides a consistent description of all experiments.

halo if the DM particles undergo elastic spin-independent scattering with $f_n/f_p = 1$. There is no functional form for $\tilde{g}(v_{\rm min})$ that would allow a DM interpretation of the CoGeNT or CRESST-II data consistent with other experiments.

4.1 A consistent description of CoGeNT and CRESST-II

Even though we cannot find a halo model that provides a consistent description of *all* experiments, it is seen from Figure 3 that CRESST-II and CoGeNT probe $\tilde{g}(v_{\rm min})$ at different ranges of $v_{\rm min}$. Therefore it should be possible to choose $\tilde{g}(v_{\rm min})$ such that we obtain a consistent description for these two experiments. This choice must be different from the SHM for which the best-fit DM regions of CRESST-II and CoGeNT do *not* overlap [16, 24].

Of course, we cannot vary $\tilde{g}(v_{\rm min})$ arbitrarily — in the end, the velocity integral must arise from a reasonable self-consistent model of the DM halo. Therefore in Figure 4, we

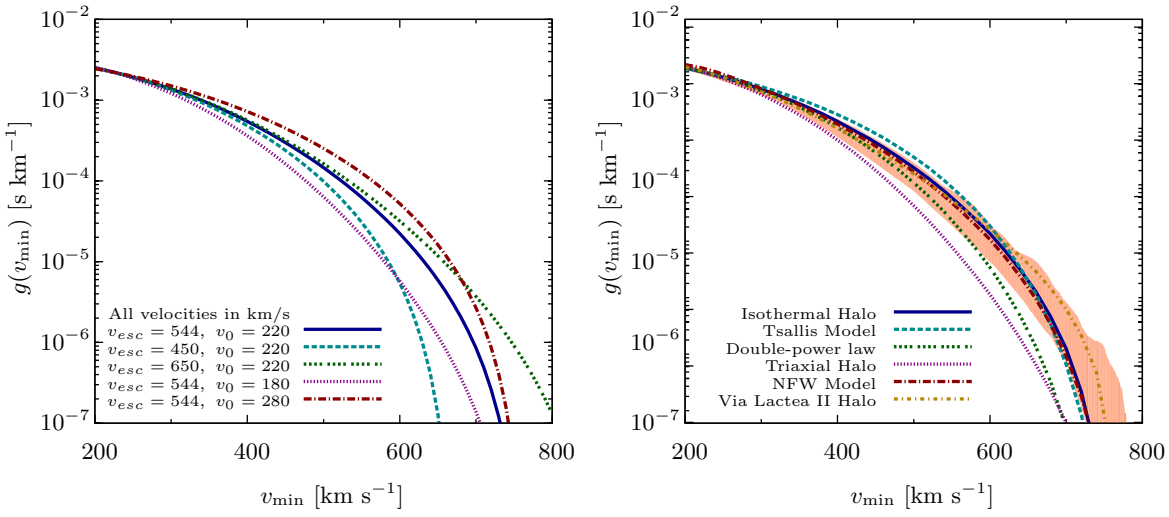


Figure 4. The velocity integral $g(v_{\rm min})$ for the SHM with different parameters (left) and alternative descriptions of the DM halo introduced in Appendix C (right). The shaded region corresponds to the values of $g(v_{\rm min})$ observed in the GHALO$_{\rm s}$ simulation [5].

examine the range of predictions for $\tilde{g}(v_{\rm min})$ from a variety of reasonable models of the galactic halo. First we note that $\tilde{g}(v_{\rm min})$ can change considerably even in the context of the SHM, if we vary v_0 and $v_{\rm esc}$ within their observational bounds (see the left panel of Figure 4). Secondly, the SHM is unlikely to be an accurate description; indeed many alternative models and parameterisations for the halo exist in the literature. We present an overview in Appendix C and show the corresponding velocity integrals in the right panel of Figure 4. Even for a fixed choice of $v_{\rm esc}$ and v_0 there is a large spread in the predictions of the velocity integral, especially close to the cut-off.

We conclude that given the spread in the predictions for $\tilde{g}(v_{\rm min})$ it should be possible to bring CoGeNT and CRESST-II into better agreement. In this context it is instructive to ask why CRESST-II favours larger DM masses than CoGeNT (see left panel of Figure 6). To understand this, we show the SHM prediction for $\tilde{g}(v_{\rm min})$ in Figure 5 together with the measurements from CoGeNT and CRESST-II for $m_\chi = 9$ GeV. We observe that the SHM prediction of the rescaled velocity integral below 500 km/s is slightly too flat to fit the CoGeNT data, thus favouring smaller DM masses. Moreover there is an additional constraint (which is not apparent in Figure 5) from the fact that CoGeNT does not observe a signal at higher energies. This constraint additionally disfavours the case $m_\chi \geq 9$ GeV if the rescaled velocity integral is too flat. Consequently if we want to push the CoGeNT region to larger DM mass, we need to make the rescaled velocity integral steeper below 500 km/s. As a result our new velocity integral will predict fewer events from oxygen in the lowest bins of CRESST-II because $\tilde{g}(v_{\rm min})$ becomes smaller around 500 km/s. To compensate, we must increase the contribution from calcium in the lowest bins, corresponding to larger values of $\tilde{g}(v_{\rm min})$ around 600 km/s (see also the discussion in Appendix A).

We can easily achieve this goal by adding two SHM-like contributions — one with relatively small velocity dispersion and low cut-off which dominates at low values of $v_{\rm min}$, and a second one with much larger v_0 and $v_{\rm esc}$. Of course, the resulting velocity distribution

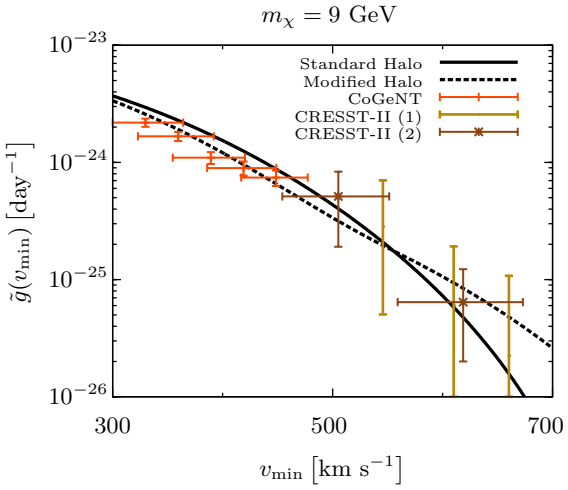


Figure 5. Measurements of the velocity integral $g(v_{\rm min})$ compared to the predictions of the SHM and the Modified Halo Model. In both cases, we have assumed $\sigma_n = 10^{-40}\,{\rm cm}^2$ and $\rho = 0.3\,{\rm GeV/cm}^3$. The Modified Halo Model provides a consistent description of the data from CoGeNT and CRESST-II for a DM particle with $m_\chi = 9$ GeV.

is *not* a self-consistent model of the DM halo; it is only a convenient parameterisation to illustrate how the velocity integral can be changed to simultaneously accommodate several direct detection experiments. Nevertheless, it is not inconceivable that such a velocity integral can be realised in models with a strong anisotropy, where the tangential component with low velocity dispersion dominates at low energies and the radial component with high dispersion dominates at high energies. We shall refer to this new velocity integral as the Modified Halo Model (MHM).

We show the corresponding best-fit regions and exclusion limits in the m_χ – σ_n plane in Figure 6. As desired, the CoGeNT and CRESST-II region[5] now overlap at $m_\chi \sim 9$ GeV. The common parameter region is, nevertheless, clearly excluded by XENON and CDMS, an observation which we could equally well have made from Figure 3.

5 Measurements and constraints for modulation amplitudes

We have seen that for all the cases considered, there is strong tension between the exclusion limits from null results and the event rate observed by CoGeNT and CRESST-II. This seems to suggest that at least some of the events seen by CoGeNT and CRESST-II may not be due to DM scattering but a new source of background [25]. We will therefore now consider a more specific signature of DM interactions, namely the annual modulation of the signal due to the motion of the Earth relative to the galactic rest frame. This will help to identify the DM signal if the background is not time-dependent.

In fact, two experiments have observed an annual modulation of their signal, namely DAMA [14] and CoGeNT [15]. By considering the modulation in $v_{\rm min}$ space, it was observed [26] that the two modulation signals are (marginally) compatible with each other, independent of astrophysics. Now we wish to include these annual modulations into our analysis of

[5]For CRESST-II we show the 1σ best-fit region using the publicly available data as stated in Appendix D. Note that this corresponds roughly to the 2σ region published by the CRESST collaboration [16].

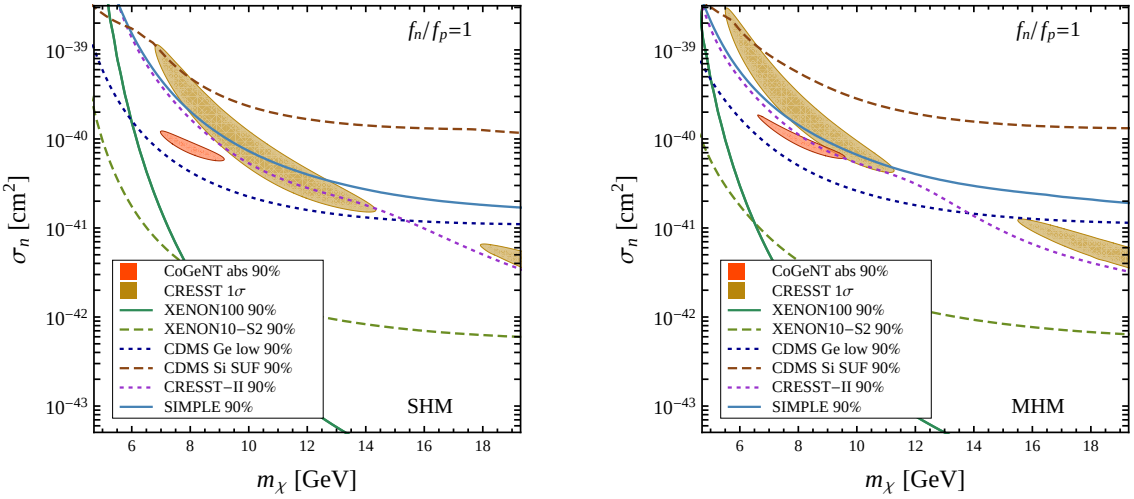


Figure 6. 90% confidence regions inferred from the absolute rate observed by CoGeNT and 1σ regions from CRESST-II as well as the 90% exclusion limits from other experiments for the SHM (left) and the Modified Halo Model (right). By construction, the Modified Halo Model leads to an overlap of the CoGeNT and CRESST-II regions.

$g(v_{\rm min})$ to determine whether these signals are compatible with the null results from other experiments. We first discuss these constraints without making any assumptions about the modulation fraction and then discuss how the modulation fraction can itself be reasonably constrained in order to obtain stronger experimental bounds.

The time dependence of $g(v_{\rm min}, t)$ can be approximately parameterised as

$$g(v_{\rm min}, t) = g(v_{\rm min}) \left[1 + A(v_{\rm min}) \cdot \cos\left(2\pi \frac{t - t_0(v_{\rm min})}{1 \text{ yr}}\right)\right] , \tag{5.1}$$

where $g(v_{\rm min})$ is the time average of $g(v_{\rm min}, t)$. Note that as emphasised earlier [5], *both* the modulation fraction A and the peak date t_0 can depend in general on $v_{\rm min}$. For future use we define the modulation amplitude $\Delta g(v_{\rm min})$ as

$$\Delta g(v_{\rm min}) \equiv \frac{1}{2}\left[g(v_{\rm min}, t_0(v_{\rm min})) - g(v_{\rm min}, t_0(v_{\rm min}) + 0.5 \text{ yr})\right] = A(v_{\rm min}) g(v_{\rm min}), \tag{5.2}$$

and introduce the rescaled modulation amplitude: $\Delta\tilde{g}(v_{\rm min}) = \Delta g(v_{\rm min})\sigma_n\rho/m_\chi$.

First we need to constrain the function $t_0(v_{\rm min})$. CoGeNT and DAMA probe largely the same region of $v_{\rm min}$ space, so it would be inconsistent to assume different phases for the two experiments. It was shown [26] that the phase measured by DAMA and by CoGeNT are consistent at the 90% confidence level for sufficiently low DM mass. We will therefore take $t_0(v_{\rm min}) = 146$ days which is the best-fit value from DAMA.[6] As the modulation fraction satisfies $A \leq 1$, we see from Eq. (5.2) that $\Delta\tilde{g}(v_{\rm min}) \leq \tilde{g}(v_{\rm min})$. We can easily check whether DAMA and CoGeNT satisfy this inequality by plotting the respective measurements of $\Delta\tilde{g}(v_{\rm min})$ on top of the constraints for $\tilde{g}(v_{\rm min})$ from other experiments which we obtained

[6] Varying t_0 within the 1σ region allowed by DAMA changes the best-fit value for the CoGeNT modulation amplitude by about 20%, which does not significantly affect any of our conclusions.

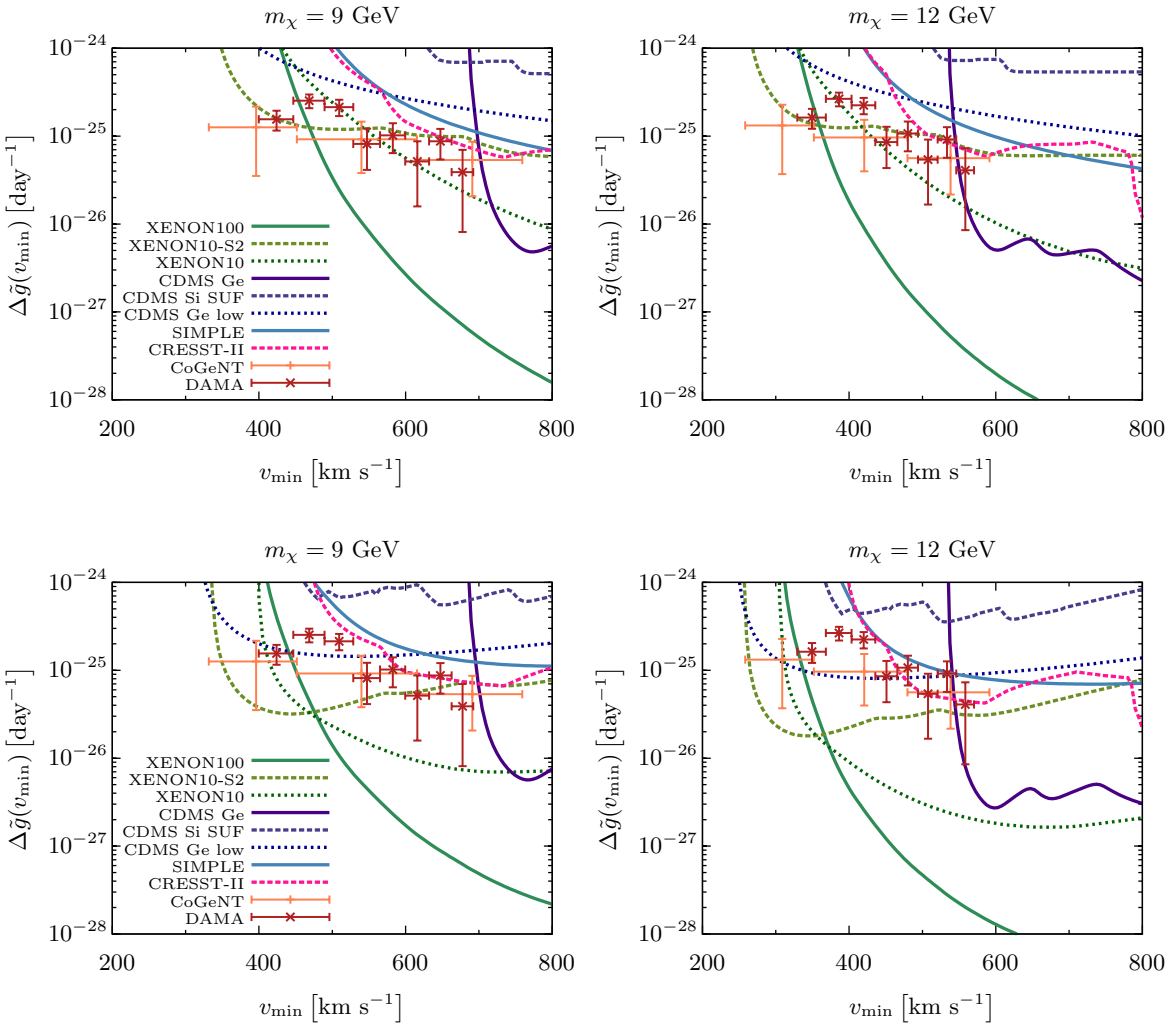


Figure 7. Measured values of $\Delta\tilde{g}(v_{\rm min})$ from DAMA and CoGeNT compared to the exclusion limits from other experiments. For the upper panels, *no* assumptions on the modulation fraction have been made, for the lower panels, we assume that the modulation fraction is bounded by the red line in the right panel of Figure 8. Even for weak assumptions on the modulation fraction, there is significant tension between the different experiments, most notably it is impossible to find a DM velocity distribution that describes the observed modulations and evades the bound from XENON100.

above. In complete analogy to Section 3.1 we can calculate $\Delta\tilde{g}(v_{\rm min})$ from the modulation of the event rate, $\Delta {\rm d}R/{\rm d}E_{\rm R}$, seen by DAMA and CoGeNT

$$\Delta\tilde{g}(v_{\rm min}) = 2\mu_{n\chi}^2 \, \frac{1}{C_{\rm T}^2(A,Z)F^2(E_{\rm R})} \, \Delta\frac{{\rm d}R}{{\rm d}E_{\rm R}} \, . \tag{5.3}$$

The resulting values of $\Delta\tilde{g}(v_{\rm min})$ are shown in Figure 7. We observe that the bounds from the XENON10 and XENON100 experiments remain strong even if we do not make any assumptions about the modulation fraction. However other experiments do not significantly constrain $\Delta\tilde{g}(v_{\rm min})$. We consider therefore whether it is reasonable to make stronger assumptions about the modulation fraction and thus obtain more stringent experimental bounds.

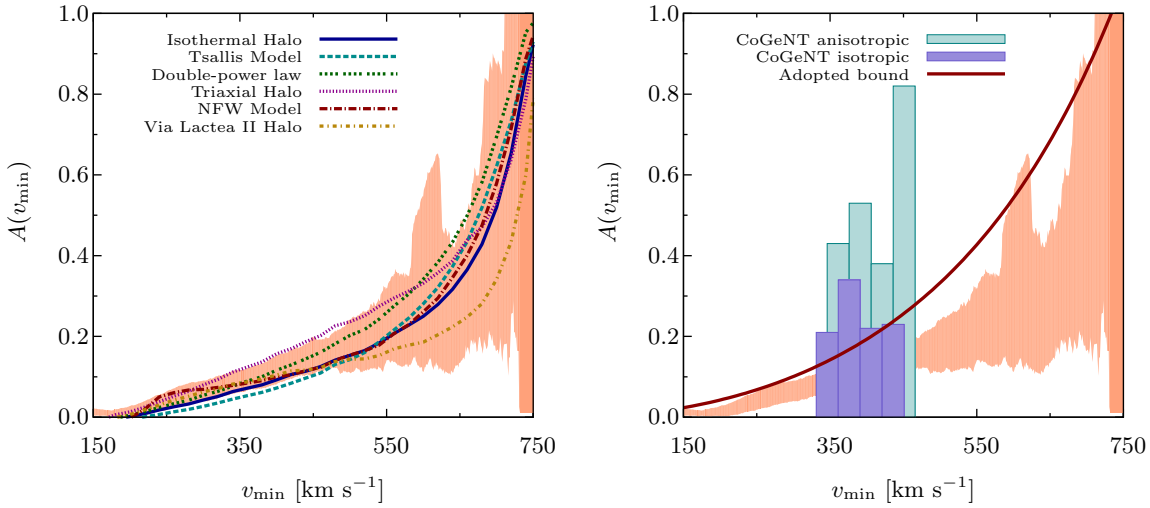


Figure 8. Left: The velocity integral and the modulation fraction for different descriptions of the galactic DM halo. Right: The constraint for the modulation fraction extracted from the CoGeNT data (boxes) together with the bound that we will adopt (red solid line). The shaded region in both panels corresponds to the modulation fractions observed in the GHALO$_{\rm s}$ simulation [5].

5.1 Constraining the modulation fraction

We will now discuss what can be reasonably assumed about the modulation fraction given known models of the galactic halo, and how it can be constrained once the velocity integral has been measured. The predicted modulation fraction for various halo models are shown in the left panel of Figure 8. We observe that for most values of $v_{\rm min}$ it is significantly below 100%. Note that a modulation fraction of 100% implies that no signal is observed at $t_0 + 0.5$ yr, which is possible only if $v_{\rm min} > v_{\rm esc} + v_{\rm E}(t_0 + 0.5\ {\rm yr})$.

The empirical bound that we will adopt is shown as the red line in the right panel of Figure 8. Note that this is a weak bound in the sense that we allow modulation fractions much larger than the value expected in any reasonable description of the DM halo. If we require that the modulation fraction satisfies $A(v_{\rm min}) \leq A^{\rm max}(v_{\rm min})$, any direct detection experiment that constrains $\tilde{g}(v_{\rm min}) \leq \tilde{g}^{\rm max}(v_{\rm min})$ will also constrain $\Delta\tilde{g}(v_{\rm min})$ according to:

$$\Delta\tilde{g}(v_{\rm min}) = A(v_{\rm min})\tilde{g}(v_{\rm min}) \leq A^{\rm max}(v_{\rm min})\tilde{g}^{\rm max}(v_{\rm min})\ . \tag{5.4}$$

The resulting measurements and constraints for $\Delta\tilde{g}(v_{\rm min})$ are shown in the lower panels of Figure 7. Even with our weak assumption concerning the modulation fraction, the bounds on $\Delta\tilde{g}(v_{\rm min})$ have become significantly stronger. Decreasing the mass of the DM particle now helps significantly because at high values of $v_{\rm min}$ larger modulation fractions are allowed so the exclusion limits become less stringent. However for small masses it becomes increasingly difficult to explain the modulation observed by CoGeNT above 2 keVee because these recoil energies correspond to very large velocities, where we expect $\tilde{g}(v_{\rm min})$ and therefore $\Delta\tilde{g}(v_{\rm min})$ to be small.

We now consider whether the modulation fraction can be constrained further using measurements of $\tilde{g}(v_{\rm min})$. Comparing the left panel of Figure 8 to the right panel of Figure 4, we observe that there is a direct correspondence between the velocity integral and the

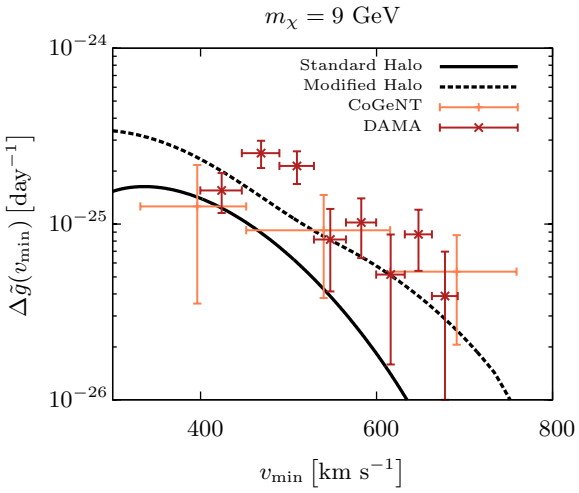


Figure 9. Measurements of the modulation amplitude $\Delta\tilde{g}(v_{\rm min})$ compared to the predictions of the SHM and the Modified Halo Model. In both cases, we have assumed $\sigma_n = 10^{-40}\,\mathrm{cm}^2$ and $\rho = 0.3$ GeV/cm^3. While in the SHM, the predicted modulation amplitude for these parameters is too small to explain the observed modulations, we can get a sufficiently large modulation amplitude in the Modified Halo Model.

modulation fraction: the steeper the slope of the velocity integral, the larger the modulation fraction. This result is intuitively clear — if $g(v_{\rm min})$ changes rapidly with varying $v_{\rm min}$ we can also expect large changes between the rates observed in summer and winter. This can in fact be used to constrain the modulation fraction once the velocity integral is known. We derive in Appendix B that

$$A(v_{\rm min}) = \frac{\tilde{g}(v_{\rm min},\ \text{summer}) - \tilde{g}(v_{\rm min},\ \text{winter})}{\tilde{g}(v_{\rm min},\ \text{summer}) + \tilde{g}(v_{\rm min},\ \text{winter})} < \frac{\tilde{g}(v_{\rm min} - u) - \tilde{g}(v_{\rm min} + u)}{2\tilde{g}(v_{\rm min})}\,, \tag{5.5}$$

where $u = 29.8$ km/s if we assume an anisotropic halo and $u = 15.0$ km/s if we assume an isotropic halo.

As an example, we can use the CoGeNT data to derive a bound on the modulation fraction for a given DM mass. For this purpose, we need to bin the measured events in such a way that the resulting bin width in $v_{\rm min}$-space is equal to u (see Appendix D). The resulting constraints are shown in the right panel of Figure 8. We observe that assuming an isotropic halo, these constraints are actually quite severe, limiting the modulation fraction to 20% at $v_{\rm min} = 400$ km/s, which in fact coincides with our adopted bound for $A(v_{\rm min})$. For an anisotropic halo, modulation fractions of up to 40% may be possible in the same range.

This observation is also relevant for a self-consistent DM interpretation of the CoGeNT experiment. To bring the modulation observed by CoGeNT into agreement with the measured event rate, a relatively large modulation fraction is required [27]. If CoGeNT were to reject a significant part of its signal as background, as suggested in Ref.[25], even larger modulation fractions will be necessary for self-consistency. The constraint on the modulation fraction derived above can then be used to conclude that the DM halo must be anisotropic.

5.2 A consistent description of DAMA and CRESST-II

As can be seen from Figure 7, DAMA and CoGeNT probe the same region of $v_{\rm min}$ space, so it is not possible to improve their agreement by changing the halo model as we did for

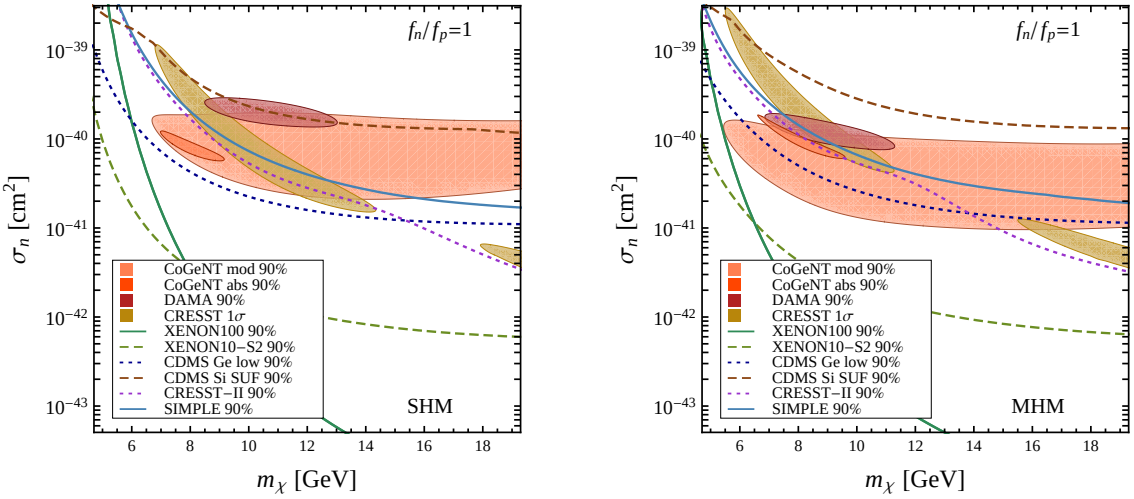


Figure 10. 90% confidence regions from CoGeNT (inferred from both the modulation and the absolute rate) as well as the 1σ region from CRESST-II and the DAMA region for the SHM (left) and the Modified Halo Model (right). The 90% exclusion limits from other experiments are also shown. By construction of the Modified Halo Model, the four best-fit regions are now in good agreement.

CoGeNT and CRESST-II. Fortunately, such a modification is not necessary because DAMA and CoGeNT favour roughly the same modulation amplitude. The more interesting question is whether this modulation amplitude is compatible with the average value of $\tilde{g}(v_{\min})$ inferred from CRESST-II and the CoGeNT unmodulated event rate.

For a cross-section of $\sigma_n \approx 10^{-40}\,\mathrm{cm}^2$, the SHM prediction of the modulation amplitude is too small to account for the modulation seen by DAMA and CoGeNT [26–30]. This is obvious from plotting the SHM prediction for $\Delta\tilde{g}(v_{\min})$ together with the measured modulation amplitudes (see Figure 9). However, we have already noted in Section 4.1 that the SHM must be modified if we want to simultaneously explain CoGeNT and CRESST-II. Now we consider if we can bring these experiments into agreement with DAMA (and therefore also with the CoGeNT modulation) by additionally allowing a larger modulation fraction. Of course, for a given velocity integral the modulation fraction must satisfy Eq. (5.5), so we cannot choose arbitrarily large values.

For this purpose, we assume that $g(v_{\min})$ is given by the Modified Halo Model from Section 4.1 and that the modulation fraction saturates the bound $A^{\max}(v_{\min})$ shown in Figure 8. By the reasoning in Appendix B these two assumptions are compatible *only* if the DM halo is highly anisotropic. As is demonstrated in Figure 9, we then obtain a sufficiently large modulation amplitude to describe the DAMA and CoGeNT modulations. Consequently, the four best-fit regions in the traditional $\sigma_n - m_\chi$ parameter plane are now in good agreement (Figure 10). However these are of course excluded by XENON and CDMS. Because of this obvious contradiction we wish to emphasise again that we do not consider present data sufficient to actually determine the velocity integral or the modulation amplitude. We use it only to illustrate how our method can be used to bring future, more reliable, data sets into agreement.

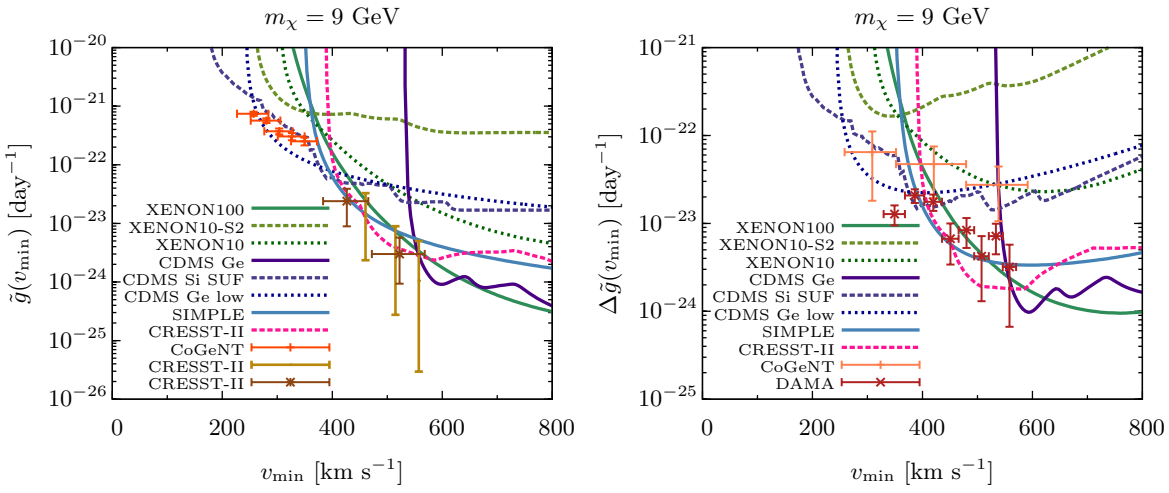


Figure 11. Measurements and exclusion bounds of the velocity integral $\tilde{g}(v_{\rm min})$ (left) and the modulation amplitude $\Delta\tilde{g}(v_{\rm min})$ (right) under the assumption $f_n/f_p = -0.7$. As above, we have assumed that the modulation fraction is bounded by the red line in the right panel of Figures 8. The bounds from liquid xenon experiments can mostly be evaded in this case but the bounds from CDMS-Si, SIMPLE, and the CRESST-II commissioning run become much more important.

5.3 Additional contributions to the local dark matter density

Our discussion of $\tilde{g}(v_{min})$ is quite independent of the origin of the local DM density. However to predict the velocity integral (Figure 4) and the modulation amplitude (Figure 8) we have assumed that the local DM density is completely dominated by the contribution from the galactic DM halo. In general there may be other significant contributions to the local DM density, e.g. from DM 'streams' and a 'dark disk'. We will now briefly discuss how these can alter the theoretical predictions of $g(v_{\rm min})$ and $A(v_{\rm min})$.

Streams

N-body simulations show that the DM velocity distribution is not a smooth function but instead has a significant amount of sub-structure [31] due to the presence of tidal streams. Such streams can have large velocities relative to the local standard of rest and can therefore contribute to $g(v_{\rm min})$ at large values of $v_{\rm min}$. The result is an edge in the velocity integral (see Figure 1) as well as a significant increase in the modulation fraction [24, 32]. Nevertheless, the bound on the modulation fraction derived in Appendix B remains valid. In other words, a large modulation fraction is always visible as a steep decrease in the velocity integral and can therefore be probed by measuring the differential event rate (see also Ref.[33] for a discussion on how to constrain DM streams with CoGeNT).

Dark disk

Most N-body simulations of the galactic DM halo neglect the effect of baryons. Baryonic matter is expected to effect the formation of a DM disk that can contribute a similar amount to the local DM density as the halo [34, 35]. Such a dark disk is expected to have a much smaller velocity dispersion than the galactic halo and to be co-rotating with only a small lag.

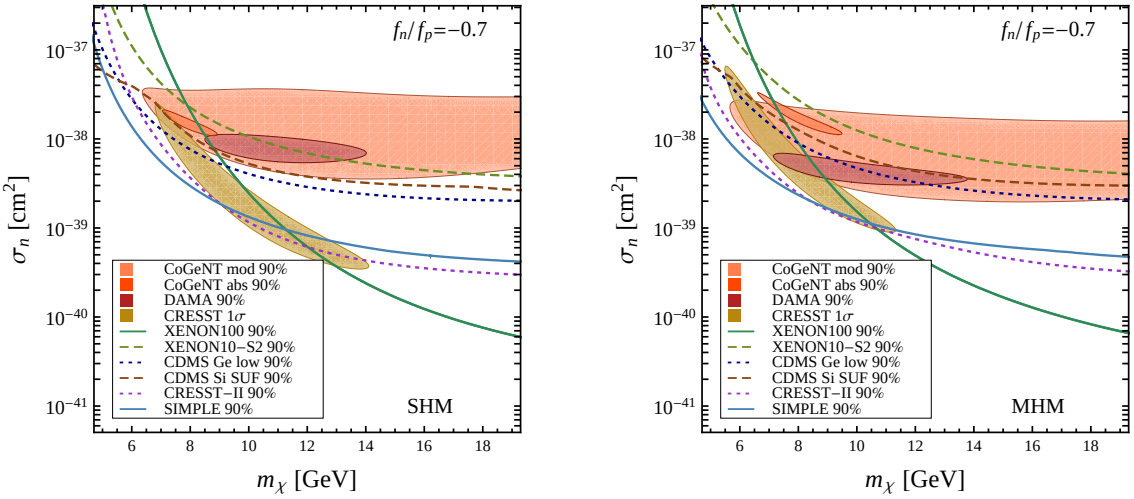


Figure 12. 90% confidence regions from CoGeNT (inferred from both the modulation and the absolute rate) as well as the 1σ region from CRESST-II and the DAMA region for the SHM (left) and the Modified Halo Model (right) for the assumption $f_n/f_p = -0.7$. The 90% exclusion limits from other experiments are also shown. For the MHM, the region of overlap from DAMA, CRESST-II and the CoGeNT modulation is only just excluded by current experimental limits.

Consequently, a dark disk will contribute to $\tilde{g}(v_{\rm min})$ only for $v_{\rm min} \leq 250$ km/s — a region that is irrelevant in the context of light DM [4, 6, 36]. For DM particles with $m_\chi > 50$ GeV, one can however expect a significant increase in both the velocity integral and the modulation fraction at low energies.

6 Varying particle physics

All the results shown so far correspond to standard assumptions for the interaction between DM particles and detector nuclei. Various modifications of these assumptions have been proposed to reduce the tension between various experiments. A particularly interesting possibility is isospin-dependent DM couplings, i.e. $f_n \neq f_p$. Choosing the ratio of couplings $f_n/f_p \simeq -0.7$ strongly suppresses the bounds from all experiments using xenon [26–30, 37–40], which are otherwise the most constraining (see Figure 10). This observation has generated much interest in DM models leading to such couplings [40–44].

We show the resulting measurements of $\tilde{g}(v_{\rm min})$ and $\Delta\tilde{g}(v_{\rm min})$ in Figure 11. The bounds from XENON10 and CDMS-Ge can be evaded in this case but the bounds from CDMS-Si, SIMPLE, and the CRESST-II commissioning run become more important. Also, for $f_n/f_p \simeq -0.7$ the agreement between CoGeNT and CRESST-II as well as the agreement between the DAMA and CoGeNT modulations get considerably worse. Interestingly, the agreement between CoGeNT and CRESST-II would improve considerably, if the CoGeNT event rate were to be reduced through to the subtraction of an additional background. The same observation can also be made from Figure 12 (see also Refs.[24, 45]). For the MHM, the region of overlap from DAMA, CRESST-II and the CoGeNT modulation is only just excluded by current experimental limits.

7 Conclusions

We have discussed how measurements of the differential event rate in nuclear recoil detectors can be used to extract information on the velocity integral $g(v_{\rm min})$. By converting experimental results into $v_{\rm min}$-space, we can compare the results from various recent DM direct detection experiments without making any assumptions concerning the properties of the DM halo. This strategy has several direct applications.

The first is to compare experiments that observe a potential DM signal with the null results from other direct detection experiments. To do this we need to translate bounds on the differential event rate into bounds on $\tilde{g}(v_{\rm min})$. In order to exclude a certain value $\tilde{g}(\hat{v}_{\rm min})$ we must demonstrate that *any* velocity integral that takes this value necessarily predicts an unacceptably large number of events in at least one of the experiments. We have utilised this approach to demonstrate that astrophysical uncertainties are *not* sufficient to solve the present conflicts between direct detection experiments. Specifically, the values of $\tilde{g}(v_{\rm min})$ favoured by CoGeNT and CRESST-II are excluded by XENON and CDMS.

The second application is to assess the compatibility of several experiments that observe a positive signal, independently of astrophysical assumptions. If the experiments probe the *same* region of $v_{\rm min}$ space, but measure contradictory values of $\tilde{g}(v_{\rm min})$, we can conclude that the two experiments cannot be brought into agreement by changing astrophysics. However, if the two experiments probe *different* regions of $v_{\rm min}$ space, either because they employ different targets or different thresholds, it will often be possible to modify the velocity integral in such a way that both experiments are brought into agreement — provided that a monotonically decreasing function fitting all data exists.

We have demonstrated this possibility by considering the recent signals seen by CoGeNT and CRESST-II. For this purpose, we have developed a method to treat targets consisting of several different nuclei. While the DM masses inferred from these measurements do not agree for the SHM, we can modify the halo model to make the respective best-fit regions overlap. To assess how reasonable such a modification of the SHM is, we have studied a large variety of different dynamical models for the galactic DM halo and calculated the respective predictions for $\tilde{g}(v_{\rm min})$. The corresponding spread in predictions for the velocity integral is rather large and justifies considering significant departures from the SHM value.

Similarly we can convert measurements of the modulation of the event rate into measurements of the modulation amplitude of the velocity integral $\Delta\tilde{g}(v_{\rm min})$. Again such a conversion can be used to check whether several experiments observing an annual modulation are compatible and to confront them with constraints from null results. We find that the annual modulations observed by CoGeNT and DAMA are consistent with each other but in conflict with the bound from XENON100 even if we allow a modulation fraction of 100%. By constraining the modulation fraction with the absolute rate we have shown that such a large modulation fraction is in fact inconsistent with the CoGeNT data. Nevertheless for anisotropic halos it remains possible to have a sufficiently large modulation fraction to allow for a consistent description of CoGeNT, DAMA and CRESST-II, although the bounds from other experiments then become much stronger.

In conclusion, for standard interactions between DM particles and nuclei, the tension between direct detection experiments cannot be completely resolved by varying astrophysical parameters. If the signals reported by DAMA, CoGeNT and CRESST-II are interpreted in terms of DM while all null results are taken at face value, non-standard interactions like isospin-dependent DM have to be invoked. We have discussed this briefly and found that

for $f_n/f_p = -0.7$ experimental constraints are significantly weaker and can be evaded by modifying the halo to have a larger modulation fraction. In this case, the CoGeNT and DAMA modulations as well as the CRESST-II event rate can be brought into agreement with all other experiments except the bound from SIMPLE and the CRESST-II commissioning run. We look forward to more data to help resolve the present puzzling situation.

Acknowledgements

We thank Wyn Evans, Matthew McCullough, John March-Russell and Andrew Brown for useful discussions and Jens Schmaler for correspondence. FK is supported by DAAD, KSH by ERC Advanced Grant (BSMOXFORD 228169) and MTF and CM by STFC grants. MTF, KSH and SS thank the CERN theory group for hospitality, especially during the TH-Institute DMUH'11 when this project was initiated. We also acknowledge support from the UNILHC network (PITN-GA-2009-237920) and an IPPP associateship for 2011-12 awarded to SS.

Appendix

A Including different target elements

As demonstrated in Section 3.1, it is relatively easy to convert energy spectra into $v_{\min}$-space for a target consisting only of a single element. However many experiments, for example SIMPLE and CRESST-II, employ a combination of different elements as target. In this case, a nuclear recoil of a given energy corresponds to different $v_{\min}$ depending on the recoiling nucleus.

We discuss how to disentangle the arising ambiguities. Note that these considerations may also be important for targets consisting of different isotopes of a single element, especially when considering isospin-dependent interactions.

A.1 Constraining the velocity integral

First, we discuss how an upper bound can be placed on the velocity integral for a null result from an experiment consisting of more than one element. The most obvious example is the SIMPLE experiment, consisting of C_2ClF_5. We apply the method presented in Section 3.1 separately to each element (or isotope) by requiring that the number of recoil events expected for this element alone does not significantly exceed the total number of events observed.

For each element we then obtain a bound $\tilde{g}^{\max}_{(i)}(v_{\min})$ on the rescaled velocity integral. We can combine these bounds into a total bound according to

$$\frac{1}{\tilde{g}^{\max}(v_{\min})} = \sum_i \frac{1}{\tilde{g}^{\max}_i(v_{\min})} \,. \tag{A.1}$$

This procedure is illustrated in Figure 13.

In fact, it is sufficient to calculate $\tilde{g}^{\max}_i(v_{\min})$ for only one of the elements in the target, as we can use this bound to infer the bounds for all other elements. Suppose we have determined the bound $\tilde{g}(v_{\min}) < \tilde{g}^{\max}_1(v_{\min})$ for $v_{\min} = \hat{v}_1$ for an isotope with charge Z_1, mass number A_1 and form factor F_1. For a different isotope, we can now infer the value of the rescaled velocity integral at the minimal velocity $\hat{v}_2$, which satisfies $E_1(\hat{v}_1) = E_2(\hat{v}_2)$, meaning that

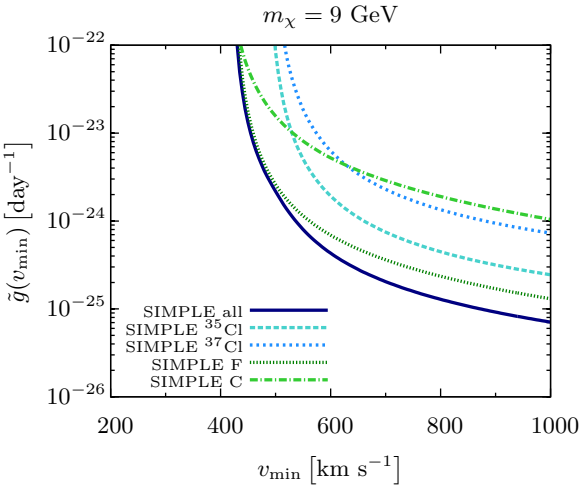


Figure 13. The individual bounds on $\tilde{g}(v_{\rm min})$ for the different elements and isotopes as well as the combined total bound from the SIMPLE experiment.

the two velocities correspond to the same maximum recoil energy on the respective nuclei. The bound from the second isotope is then given by

$$\tilde{g}_2^{\rm max}(\hat{v}_2) = \frac{c_1 C_{\rm T}^2(Z_1, A_1) F_1(E_1(\hat{v}_1))^2}{c_2 C_{\rm T}^2(Z_2, A_2) F_2(E_2(\hat{v}_2))^2} \tilde{g}_1^{\rm max}(\hat{v}_1) \,, \tag{A.2}$$

where $c_{1,2}$ are the respective concentrations of the isotopes.

A.2 Measuring the velocity integral

We turn now to the more difficult task of inferring information on $\tilde{g}(v_{\rm min})$ from a potential DM signal in an experiment consisting of several different elements. The obvious application is the CRESST-II experiment, which we will use here for illustration. We consider only the contribution of calcium and oxygen, because for DM masses of 15 GeV and less, nuclear recoils on tungsten have recoil energies well below the threshold of the detector.

The differential event rate in CRESST-II is given by the sum of the differential event rates for the individual elements, i.e.

$$\left(\frac{{\rm d}R}{{\rm d}E_{\rm R}}\right)^{\rm tot} = \left(\frac{{\rm d}R}{{\rm d}E_{\rm R}}\right)^{\rm (O)} + \left(\frac{{\rm d}R}{{\rm d}E_{\rm R}}\right)^{\rm (Ca)} \,. \tag{A.3}$$

To cause a recoil of energy $E_{\rm R}$, a DM particle must have a minimum velocity of $v_{\rm min}^{\rm (O)}(E_{\rm R})$ for scattering off oxygen and $v_{\rm min}^{\rm (Ca)}(E_{\rm R})$ for calcium. Consequently, if we measure the differential event rate at the energy $E_{\rm R}$, we simultaneously probe the rescaled velocity integral at *both* of these velocities. Therefore, we can only extract information on $\tilde{g}(v_{\rm min}^{\rm (O)}(E_{\rm R}))$ if we know the ratio of the differential event rates for scattering off oxygen and calcium

$$\frac{({\rm d}R/{\rm d}E_{\rm R})^{\rm (O)}}{({\rm d}R/{\rm d}E_{\rm R})^{\rm (Ca)}} = \frac{C_{\rm T}^2(Z^{\rm (O)}, A^{\rm (O)}) \cdot F^{\rm (O)}(E_{\rm R})^2 \cdot g(v_{\rm min}^{\rm (O)}(E_{\rm R}))}{C_{\rm T}^2(Z^{\rm (Ca)}, A^{\rm (Ca)}) \cdot F^{\rm (Ca)}(E_{\rm R})^2 \cdot g(v_{\rm min}^{\rm (Ca)}(E_{\rm R}))} \,. \tag{A.4}$$

We present two different methods to determine this ratio. The first makes use of the fact that the rescaled velocity integral is a decreasing function of $v_{\rm min}$ to place an upper bound on

the contribution from calcium. The second method requires a special binning of the data in such a way that the contribution of calcium can actually be determined from the combined information of several bins. Once we have an estimate of the differential event rate from oxygen alone, we can use the procedure described in Section 3.1 to obtain the corresponding values of $\tilde{g}(v_{\rm min})$.

Method 1

This method makes use of the fact that $v_{\rm min}^{\rm (Ca)} > v_{\rm min}^{\rm (O)}$ for the same recoil energy, because calcium is the heavier nucleus and we are only interested in the case where $m_\chi < m_{\rm O}$. We know that $\tilde{g}(v_{\rm min})$ must decrease as $v_{\rm min}$ increases, so $g(v_{\rm min}^{\rm (Ca)}(E_{\rm R})) < g(v_{\rm min}^{\rm (O)}(E_{\rm R}))$. Substituting this expression into Eq. (A.4), it is possible to place a lower bound on the contribution of oxygen

$$\left(\frac{{\rm d}R}{{\rm d}E_{\rm R}}\right)^{\rm (O)} > \frac{C_{\rm T}^2(Z^{\rm (O)},A^{\rm (O)})\cdot F^{\rm (O)}(E_{\rm R})^2}{C_{\rm T}^2(Z^{\rm (Ca)},A^{\rm (Ca)})\cdot F^{\rm (Ca)}(E_{\rm R})^2}\left(\frac{{\rm d}R}{{\rm d}E_{\rm R}}\right)^{\rm (Ca)} \equiv S^{\rm (O,Ca)}(E_{\rm R})\left(\frac{{\rm d}R}{{\rm d}E_{\rm R}}\right)^{\rm (Ca)} \quad \text{(A.5)}$$

If the differential event rate $({\rm d}R/{\rm d}E_{\rm R})^{\rm tot}$ is known, we can make use of this inequality and Eq. (A.3) to infer that

$$\left(\frac{{\rm d}R}{{\rm d}E_{\rm R}}\right)^{\rm (O)} > \left(\frac{{\rm d}R}{{\rm d}E_{\rm R}}\right)^{\rm tot}\frac{S^{\rm (O,Ca)}(E_{\rm R})}{1+S^{\rm (O,Ca)}(E_{\rm R})}\,. \quad \text{(A.6)}$$

In practice, additional factors like the target composition and the acceptance for each nuclear recoil need to be included in $S^{\rm (O,Ca)}(E_{\rm R})$. In the case of CRESST-II, the minimum contribution of oxygen in the relevant energy region is approximately 20%.

Note, that this method only constrains, but does not actually determine, the ratio of oxygen to calcium scatters in each bin. The lower bound that we obtain is almost independent of energy although we expect the oxygen fraction to approach 100% as the recoil energy increases. To reflect our ignorance of the true ratio, we do not show central values for the measurements of $\tilde{g}(v_{\rm min})$ obtained with this method. The second method, which we present below, will allow for a more accurate determination of the ratio of oxygen to calcium scatters.

Method 2

In the approach discussed above, we considered each bin separately and treated the presence of a second (heavier) element in the target as an additional uncertainty which reduces the information that we can extract from the data on the velocity integral. It would be desirable to develop a method that combines the information from different bins in order to use *both* target elements to and constrain the velocity integral more tightly. We now present such a method.

First of all, we must construct energy bins of different sizes according to the following rule: Starting from an arbitrary bin $\left[E_1^{\rm min}, E_1^{\rm max}\right]$, we use the heavier target (assumed to be calcium) to convert the boundaries into $v_{\rm min}$-space and then the lighter target (oxygen) to convert the velocities back into energy space. This way, we obtain a new energy bin $\left[E^{\rm (O)}(v_{\rm min}^{\rm (Ca)}(E_1^{\rm min})), E^{\rm (O)}(v_{\rm min}^{\rm (Ca)}(E_1^{\rm max}))\right]$. The two bins thus constructed have the property that calcium recoils with energies in bin 1 probe the *same* region of $v_{\rm min}$-space as oxygen recoils with energies in bin 2. We can repeat this procedure recursively to obtain additional bins with increasing bin size (see Figure 14). It is always possible to choose the first bin in such a way that the different bins do not overlap.

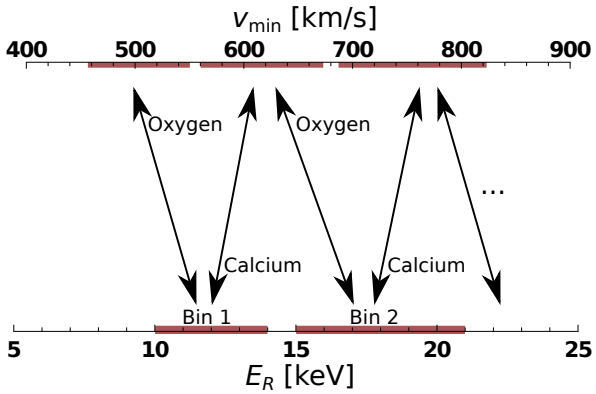


Figure 14. An illustration of the method used to construct bins for CRESST-II. The two bins constructed in this way have the property that calcium recoils with energies in bin 1 probe the *same* region of $v_{\rm min}$-space as oxygen recoils with energies in bin 2. For this plot, we have assumed $m_\chi = 9$ GeV.

We only wish to consider bins where a significant excess of signal over expected background is observed, meaning that we abort the iteration as soon as we obtain a bin where the signal is compatible with the background estimate. To give a concrete example, for $m_\chi = 9$ GeV the energy conversion factor between oxygen and calcium is

$$\frac{m_{\rm Ca}}{\mu^2_{\rm Ca}} \frac{\mu^2_{\rm O}}{m_{\rm O}} = 1.50 \,, \tag{A.7}$$

so a possible construction for an experiment like CRESST-II would be [8 keV, 12 keV], [12 keV, 18 keV], [18 keV, 27 keV]. Unfortunately, the current CRESST-II data reaches down only to 10 keV and we cannot bin the data arbitrarily so we will use only the two bins [10 keV, 14 keV] and [15 keV, 21 keV] here. For different values of m_χ the conversion factor will also change, so different bins must be considered. We present possible choices for different DM masses in Table 1.

We start by evaluating the highest bin and then work our way back towards bin 1. In the highest bin, we can reasonably assume that the observed event rate is completely dominated by the lightest element in the target. The reason is that we expect events in this bin to arise from DM particles close to the escape velocity (otherwise, there would also be events in higher energy bins). Consequently, in the corresponding region of $v_{\rm min}$-space, we expect the velocity integral to decrease rapidly with increasing $v_{\rm min}$ (see Figure 4) so that a lighter target element should have a much larger event rate than a heavier one (probing the velocity integral at higher velocities).

This assumption is good under two conditions. First, that the different target nuclei are not too close in mass so that they actually probe different regions of $v_{\rm min}$-space and second, that there is no additional source of background at large energies that can hide a potential signal in higher energy bins. Both of these conditions are fulfilled for the CRESST-II experiment, where the background at large energies is approximately flat.

Under the assumption that only the lightest element contributes in the highest bin, we can calculate $\tilde{g}(v_{\rm min})$ for this bin in the same way as described in Section 3.1 for a target consisting of a single element. Now we can exploit the fact that we have constructed the bins

m_χ / GeV	Conversion factor	Bin 1 / keV	Bin 2 / keV
6	1.72	10 – 14	17 – 24
9	1.50	10 – 14	15 – 21
12	1.34	12 – 15	16 – 20
15	1.22		

Table 1. The energy conversion factors between oxygen recoils and calcium recoils for constant $v_{\rm min}$ for different choices of the DM mass m_χ. The third and fourth column give possible choices for two bins that are related by this conversion factor. For $m_\chi = 15$ GeV, a different binning of the CRESST-II data would be required to construct non-overlapping bins.

in a special way and use the inferred value of $\tilde{g}(v_{\rm min})$ to *predict* the number of calcium events in the next lower bin.

We can then subtract the predicted number of calcium events in the next lower bin to obtain the number of events that is due to oxygen scatters alone. Again, we are left with a number of events that correspond to scattering of the lightest element alone. We can use this number to calculate $\tilde{g}(v_{\rm min})$ in the region of $v_{\rm min}$-space corresponding to the second to highest bin. Using this measurement to predict the calcium scatters in the next lower bin, we can recursively extract $\tilde{g}(v_{\rm min})$ for all bins. Compared to the previous method, the advantage is clearly a much more accurate prediction of $\tilde{g}(v_{\rm min})$. The disadvantage is that we are forced to bin the data in a certain way, which is inconvenient if the energy of each event is not publicly available.

B Constraining the modulation fraction using the absolute rate

We will demonstrate that it is possible to constrain the modulation fraction once we have determined the average value of the rescaled velocity integral from a direct detection experiment, without assuming any specific properties of the DM halo. The basic idea is that we can place an upper bound on the maximum value, $\tilde{g}(v_{\rm min},\ \text{summer})$, and a lower bound on the minimum value, $\tilde{g}(v_{\rm min},\ \text{winter})$, using only the time average, $\tilde{g}(v_{\rm min})$.

How such bounds can be obtained is sketched in Figure 15. We observe that

$$\tilde{g}(v_{\rm min},\ \text{summer}) < \tilde{g}(v_{\rm min} - u) \tag{B.1}$$

$$\tilde{g}(v_{\rm min},\ \text{winter}) > \tilde{g}(v_{\rm min} + u) \tag{B.2}$$

where $u = 29.8$ km/s is the velocity of the Earth around the Sun. From this it follows that

$$\Delta\tilde{g}(v_{\rm min}) = \tilde{g}(v_{\rm min},\ \text{summer}) - \tilde{g}(v_{\rm min},\ \text{winter}) < \tilde{g}(v_{\rm min} - u) - \tilde{g}(v_{\rm min} + u), \tag{B.3}$$

and therefore, that the modulation fraction is bounded by

$$A(v_{\rm min}) = \frac{\tilde{g}(v_{\rm min},\ \text{summer}) - \tilde{g}(v_{\rm min},\ \text{winter})}{\tilde{g}(v_{\rm min},\ \text{summer}) + \tilde{g}(v_{\rm min},\ \text{winter})} < \frac{\tilde{g}(v_{\rm min} - u) - \tilde{g}(v_{\rm min} + u)}{2\tilde{g}(v_{\rm min})}, \tag{B.4}$$

where we have used $\tilde{g}(v_{\rm min},\ \text{summer}) + \tilde{g}(v_{\rm min},\ \text{winter}) \approx 2\tilde{g}(v_{\rm min})$.

Note that an even stronger constraint can be obtained under the assumption of an isotropic DM halo. In this case, only the seasonal change in the *radial* component of $\boldsymbol{u}$, u_r, matters, because the halo will look the same for any value of u_ϕ and u_θ. In this case, we can replace u by $u_r = u\cos\gamma = 15.0$ km/s in the equation above, where γ is the inclination angle between the galactic and ecliptic plane.

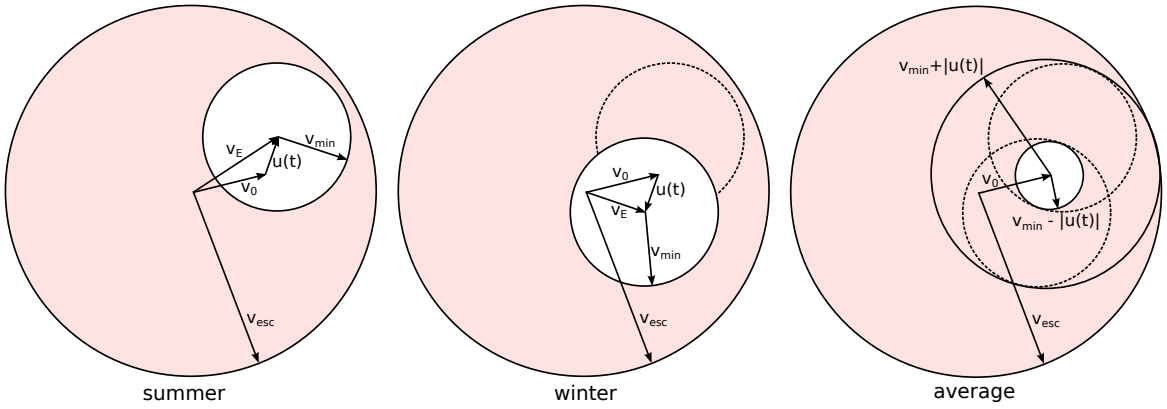


Figure 15. A graphical representation of the velocity integral. The red shaded region is the region of velocity space that is being integrated over, while the white regions are excluded by the requirement $v > v_{\rm min}$. We can place an upper bound on the maximum value, $\tilde{g}(v_{\rm min},\ \text{summer})$, and a lower bound on the minimum value, $\tilde{g}(v_{\rm min},\ \text{winter})$, using only the time average, $\tilde{g}(v_{\rm min})$. Note that the relative magnitude of the different velocities are not drawn to scale.

C Various descriptions of the DM halo

We present the velocity distributions considered in Sections 4 and 5 and provide the parameter choices used for Figures 4 and 8 — for further details see the references. First, we discuss isotropic velocity distributions, where $f(\boldsymbol{v})$ depends only on $|\boldsymbol{v}|$ and there is no preferred direction for DM velocities at the position of the Earth. Then we consider models where the anisotropy parameter

$$\beta(r) \equiv 1 - \frac{\langle v_\theta^2 \rangle + \langle v_\phi^2 \rangle}{2\langle v_r^2 \rangle} \tag{C.1}$$

is non-zero, motivated by numerical simulations which favour radially biased orbits with $\beta = 0.1 - 0.4$ at the position of the Earth.

C.1 Isotropic models

Standard Halo Model

In the Standard Halo Model (SHM), the velocity distribution function is given by

$$f(\boldsymbol{v}) = \begin{cases} \frac{1}{N}\left[\exp(-v^2/v_0^2) - \exp(-v_{\rm esc}^2/v_0^2)\right] & |\boldsymbol{v}| < v_{\rm esc} \\ 0 & |\boldsymbol{v}| \geq v_{\rm esc} \end{cases}, \tag{C.2}$$

where N is a normalisation constant. Possible values for the velocity dispersion v_0 range from 180 km/s to 280 km/s, while $v_{\rm esc}$ can vary between 450 km/s and 650 km/s (see also the left panel of Figure 4). Unless explicitly stated otherwise, we will always assume the standard values $v_0 = 220$ km/s and $v_{\rm esc} = 544$ km/s.

King models

The cut-off at $v_{\rm esc}$ is introduced by hand in the SHM, which would otherwise predict particles with infinitely high velocities and an infinite mass for the Galaxy. This problem is

addressed in the King model, which provides a cut-off in a self-consistent manner. The velocity distribution is obtained from the distribution function:

$$f(\mathcal{E}) = \begin{cases} \frac{1}{N}\left[\exp\left(\mathcal{E}/\sigma^2\right) - 1\right], & \mathcal{E} > 0 \\ 0, & \mathcal{E} \leq 0 \end{cases}, \tag{C.3}$$

where $\mathcal{E} = \Psi(\boldsymbol{x}) - v^2/2$ and $\Psi(\boldsymbol{x})$ is the relative gravitational potential. The local escape velocity at a position $\boldsymbol{x}$ is given by $v_{\rm esc} = \sqrt{2\Psi(\boldsymbol{x})}$. At the position of the Earth $f(\boldsymbol{v})$ can be parameterised in the same way as the SHM but the parameter σ is not directly linked to the velocity dispersion and can therefore take values that are much larger than in the SHM [46, 47]. Nevertheless, due to its similarity to the SHM we will not discuss King models further.

Double power-law profiles

A simple modification of the SHM was introduced in Ref.[48]. For double power-law density profiles such as the NFW-profile [49], the following ansatz for the velocity distribution reproduces better the behaviour at high velocities:

$$f(\boldsymbol{v}) = \begin{cases} \frac{1}{N}\left[\exp\left(\frac{v_{\rm esc}^2 - v^2}{k v_0^2}\right) - 1\right]^k, & |\boldsymbol{v}| < v_{\rm esc} \\ 0, & |\boldsymbol{v}| \geq v_{\rm esc} \end{cases}. \tag{C.4}$$

Setting the power-law index k equal to 1 recovers the SHM. The choice $1.5 \leq k \leq 3.5$ is found to give a better fit to velocity distributions extracted from N-body simulations. We use $k = 2.5$ throughout.

Tsallis model

It was argued [34] that the velocity distribution of dark matter particles in numerical simulations including baryons can be well described by

$$f(\boldsymbol{v}) = \begin{cases} \frac{1}{N}\left[1 - (1-q)\,\frac{\boldsymbol{v}^2}{v_0^2}\right]^{1/(1-q)}, & |\boldsymbol{v}| < v_{\rm esc} \\ 0, & |\boldsymbol{v}| \geq v_{\rm esc} \end{cases}, \tag{C.5}$$

see also Ref.[50]. We adopt the parameters $q = 0.773$, $v_0 = 267.2$ km/s and $v_{\rm esc} = 560.8$ km/s from Ref.[34].

C.2 Anisotropic models

Numerical simulations

A simple anisotropic model has been proposed [5] to describe the data from numerical N-body simulations such as Via Lactea [51, 52], GHALO [53] or Aquarius [54]:

$$f(\boldsymbol{v}) = \begin{cases} \frac{1}{N}\left[\exp\left(-(v_r^2/\overline{v}_r^2)^{\alpha_r}\right)\exp\left(-(v_t^2/\overline{v}_t^2)^{\alpha_t}\right)\right], & |\boldsymbol{v}| < v_{\rm esc} \\ 0, & |\boldsymbol{v}| \geq v_{\rm esc} \end{cases}, \tag{C.6}$$

where $v_t = \sqrt{v_\theta^2 + v_\phi^2}$. For the figures we take the best-fit parameters for the Via Lactea II simulation, namely $v_r = 202.4$ km/s, $v_t = 128.9$ km/s, $\alpha_r = 0.934$ and $\alpha_t = 0.642$ [5], but we also show the velocity integral and modulation fraction observed in the GHALO$_{\rm s}$ simulation.

Logarithmic ellipsoidal model

The simplest triaxial generalisation of the velocity distributions considered above was discussed in Refs.[2, 55, 56]. We allow a different velocity dispersion in all three directions, giving

$$f(\boldsymbol{v}) = \begin{cases} \frac{1}{N}\left[\exp\left(-v_r^2/\overline{v}_r^2 - v_\phi^2/\overline{v}_\phi^2 - v_z^2/\overline{v}_z^2\right)\right], & |\boldsymbol{v}| < v_{\rm esc} \\ 0, & |\boldsymbol{v}| \geq v_{\rm esc} \end{cases} . \tag{C.7}$$

The three parameters $\overline{v}_r$, $\overline{v}_\phi$ and $\overline{v}_z$ depend on two constants p and q that describe the density distribution and the isotropy parameter γ (as well as v_0). Following Ref.[2], we take $p = 0.9$, $q = 0.8$ and $\gamma = -1.33$ and calculate $\overline{v}_r$, $\overline{v}_\phi$ and $\overline{v}_z$ under the assumption that the Earth is on the major axis.

Distribution functions with $\beta = 0.5$

For a constant anisotropy of $\beta = 0.5$, it is possible to calculate the velocity distribution from a given density profile. This was done [57], for centrally cusped density profiles of the form

$$\rho \propto \frac{a^{b-2}}{r(r+a)^{b-1}} . \tag{C.8}$$

For example, for $b = 4$, corresponding to the Hernquist density profile [58], the velocity profile is given by

$$f(\boldsymbol{v}) = \begin{cases} \frac{1}{N}\frac{1}{v_{\rm esc}\sqrt{v_x^2+v_y^2}}\left(1 - \frac{v_x^2+v_y^2+v_z^2}{v_{\rm esc}^2}\right)^2, & |\boldsymbol{v}| < v_{\rm esc} \\ 0, & |\boldsymbol{v}| \geq v_{\rm esc} \end{cases} . \tag{C.9}$$

For $b = 3$, corresponding to the NFW profile [49], an analytical expression of the velocity distribution does not exist, but it is straightforward to numerically calculate the velocity distribution from the density profile. For the plots shown we adopt $a = 10$ kpc.

D Overview of direct detection experiments

We will briefly discuss the direct detection experiments that we have considered in this paper and state the assumptions that we have made. To derive constraints from XENON100, XENON10, CDMS-Ge and CRESST-II, we employ the 'maximum gap' method [59], while for the low threshold analysis of CDMS-Ge and CDMS-Si, we use the 'binned Poisson' method [60, 61]. Our best-fit regions are calculated using a χ^2 parameter estimation method.[7]

XENON100

We use the most recent data from 100.9 live days of data taking [17]. For the relative scintillation efficiency $\mathcal{L}_{\rm eff}$ we use a logarithmical extrapolation to zero and calculate the energy resolution under the assumption that it is dominated by Poisson fluctuations in the number of photoelectrons.

[7] For CRESST-II we use Eq. (13) from Ref.[3] to calculate the best-fit parameter region.

Bin / keVee	Event rate in cpd kg^{-1} keVee^{-1}	Error in cpd kg^{-1} keVee^{-1}
0.50 – 0.61	12.8	1.0
0.61 – 0.72	10.1	0.9
0.72 – 0.85	6.7	0.8
0.85 – 1.00	5.5	0.8
1.00 – 1.15	4.5	0.7
Bin / keVee	Modulation amplitude in cpd kg^{-1} keVee^{-1}	Error in cpd kg^{-1} keVee^{-1}
0.5 – 1.0	0.75	0.54
1.0 – 2.0	0.51	0.30
2.0 – 3.2	0.26	0.16

Table 2. The CoGeNT event rate and its modulation: the modulation amplitude has been obtained by fitting a cosine with period fixed to 365 days and the phase fixed to $t_0 = 146$ days.

XENON10

It is important to note that the published XENON10 data from Ref.[62] was based on outdated assumptions concerning the relative scintillation efficiency, so all energy scales must be rescaled to the same $\mathcal{L}_{\rm eff}$ as for the XENON100 data. We calculate the energy resolution in the same way as for XENON100.

We also consider the $S2$-only analysis presented in Ref.[63]. We adopt their conservative assumption for the ionisation yield with a sharp cut-off at 1.4 keV and take a flat detector acceptance of 0.41. To calculate the energy resolution we assume that the production of electrons is governed by Poisson statistics. We also apply the z-cut suggested by the XENON10 collaboration to reduce the number of observed events.

CoGeNT

We analyse the publicly available data from the CoGeNT experiment over the course of 1.2 years [15]. To determine the total event rate, we subtract the L-shell EC contribution and a constant background. We use the Lindhard quenching factor and the (corrected) detector resolution from Ref.[69]. The efficiency curve was provided by J. Collar (private communication). Our bin width is 0.05 keVee.

To determine the modulation, we fix the peak date to $t_0 = 146$ days, which is the best-fit value for the DAMA modulation. The bins considered and the resulting event rates and modulation amplitudes are given in Table 2.

CDMS-Ge

We use the final data [18] corresponding to an exposure of 612 kg days. We assume a detector resolution of 0.4 keV and take the detector acceptance from Ref.[64].

We also consider the dedicated low-threshold analysis of the CDMS-Ge data [19] and use only the data of the most constraining detector, T1Z5. Here, we adopt an energy resolution of $0.2\,(E_{\rm R}\cdot{\rm keV})^{1/2}$ [65].

CDMS-Si

To obtain a constraint from the silicon detectors in CDMS-II, we take the low-threshold data from the shallow-site run [66]. We include the runs at 3V and at 6V but consider only the Z4

Bin / keV	Total events	Expected background	Signal (min)	Signal (max)
10 – 13	9	3.2	3.2	9.6
13 – 16	15	6.1	5.3	13.3
16 – 19	11	7.0	1.2	7.8
19 – 22	8	6.3	0.2	5.0
22 – 25	4	5.2	0	1.8
25 – 28	4	4.6	0	2.2
28 – 31	4	4.3	0	2.5
31 – 34	3	4.0	0	1.5
34 – 37	4	3.7	0	3.0
37 – 40	5	3.5	0.2	4.3
13 – 15	11	3.8	4.0	11.0
16 – 19	11	7.0	1.2	7.8
19 – 22	8	6.3	0.2	5.0
10 – 14	18	5.4	8.4	17.4
12 – 15	19	5.7	9.1	18.1
15 – 21	19	13.7	1.7	10.1
16 – 20	13	9.4	0.9	7.9
17 – 24	17	14.1	0.5	7.7

Table 3. Data from the CRESST-II experiment: total number of events, expected number of background events and 1σ confidence interval for the signal using a Feldman-Cousins approach.

detector which gives the strongest bound. Resolution and detector efficiency are both taken from Ref.[66].

SIMPLE

We do not attempt to combine the results from Stage 1 [67] and Stage 2 [68] but consider only the latter. Since the recoil energy is not measured, the experiment can place only an upper limit on the total event rate above the detector threshold of 8 keV. We take the cut acceptance and nucleation efficiency from Ref.[68].

CRESST-II

We use the recent results from 730 kg days of data taking [16]. We estimate that the acceptance region corresponds to 86% acceptance for oxygen, 89% for tungsten and 90% for calcium. We take the energy resolution to be 0.3 keV for each detector. To extract the DM signal, we read off the total number of measured events and the expected background from Figure 11 of Ref.[16] and use the Feldman-Cousins approach [70].

Depending on the application, we bin the CRESST-II data in different ways. In order to calculate best-fit parameter regions, we consider a bin width of 3 keV, rather than a bin width of 1 keV as presented in Ref.[16]. However, if we want to calculate $\tilde{g}(v_{\rm min})$ using Method 1 from Appendix A.2, we have to make sure that the detector efficiency does not vary strongly within a single bin due to the onset of additional detector modules. This condition is fulfilled for the three bins [13 keV – 15 keV], [16 keV – 19 keV] and [19 keV – 22 keV]. Finally, to apply Method 2 from Appendix A.2, we need to bin the data in a special way, namely in the two bins [10 keV – 14 keV] and [15 keV – 21 keV]. The resulting number of events is shown in Table 3.

Finally, we also consider the improved constraint from the CRESST-II commissioning run presented in Ref.[71] using the detector efficiencies given there.

DAMA

We use the combined observed event rates from DAMA/NaI and DAMA/LIBRA [14] for the 8 bins spanning the energy range 2-6 keVee. No significant modulation is observed at higher energies. As we are interested in DM particles with mass below 20 GeV, we neglect scattering on iodine and consider only the contribution of sodium. We assume a quenching factor of 0.3 (other values are discussed in Refs.[24, 45]) and no contribution from channelling [72].

References

[1] M. Kamionkowski and A. Kinkhabwala, *Galactic halo models and particle dark matter detection*, *Phys.Rev.* **D57** (1998) 3256–3263, [hep-ph/9710337].

[2] A. M. Green, *Effect of halo modeling on WIMP exclusion limits*, *Phys.Rev.* **D66** (2002) 083003, [astro-ph/0207366].

[3] M. Fairbairn and T. Schwetz, *Spin-independent elastic WIMP scattering and the DAMA annual modulation signal*, *JCAP* **0901** (2009) 037, [arXiv:0808.0704].

[4] J. March-Russell, C. McCabe, and M. McCullough, *Inelastic Dark Matter, Non-Standard Halos and the DAMA/LIBRA Results*, *JHEP* **05** (2009) 071, [arXiv:0812.1931].

[5] M. Kuhlen *et. al.*, *Dark Matter Direct Detection with Non-Maxwellian Velocity Structure*, *JCAP* **1002** (2010) 030, [arXiv:0912.2358].

[6] A. M. Green, *Dependence of direct detection signals on the WIMP velocity distribution*, *JCAP* **1010** (2010) 034, [arXiv:1009.0916].

[7] L. E. Strigari and R. Trotta, *Reconstructing WIMP Properties in Direct Detection Experiments Including Galactic Dark Matter Distribution Uncertainties*, *JCAP* **0911** (2009) 019, [arXiv:0906.5361].

[8] C. McCabe, *The Astrophysical Uncertainties Of Dark Matter Direct Detection Experiments*, *Phys.Rev.* **D82** (2010) 023530, [arXiv:1005.0579].

[9] C. Arina, J. Hamann, and Y. Y. Wong, *A Bayesian view of the current status of dark matter direct searches*, *JCAP* **1109** (2011) 022, [arXiv:1105.5121].

[10] A. H. Peter, *WIMP astronomy with liquid-noble and cryogenic direct-detection experiments*, *Phys.Rev.* **D83** (2011) 125029, arXiv:1103.5145.

[11] M. Drees and C.-L. Shan, *Reconstructing the Velocity Distribution of WIMPs from Direct Dark Matter Detection Data*, *JCAP* **0706** (2007) 011, [astro-ph/0703651].

[12] P. J. Fox, J. Liu, and N. Weiner, *Integrating Out Astrophysical Uncertainties*, *Phys.Rev.* **D83** (2011) 103514, [arXiv:1011.1915].

[13] M. Drees and C.-L. Shan, *Model-Independent Determination of the WIMP Mass from Direct Dark Matter Detection Data*, *JCAP* **0806** (2008) 012, [arXiv:0803.4477].

[14] R. Bernabei, P. Belli, F. Cappella, R. Cerulli, C. Dai, *et. al.*, *New results from DAMA/LIBRA*, *Eur.Phys.J.* **C67** (2010) 39–49, [arXiv:1002.1028].

[15] C. Aalseth, P. Barbeau, J. Colaresi, J. Collar, J. Leon, *et. al.*, *Search for an Annual Modulation in a P-type Point Contact Germanium Dark Matter Detector*, *Phys.Rev.Lett.* **107** (2011) 141301, arXiv:1106.0650.

[16] G. Angloher, M. Bauer, I. Bavykina, A. Bento, C. Bucci, *et. al.*, *Results from 730 kg days of the CRESST-II Dark Matter Search*, arXiv:1109.0702.

[17] **XENON100 Collaboration** Collaboration, E. Aprile *et. al.*, *Dark Matter Results from 100 Live Days of XENON100 Data*, *Phys.Rev.Lett.* **107** (2011) 131302, [arXiv:1104.2549].

[18] **The CDMS-II** Collaboration, Z. Ahmed *et. al.*, *Dark Matter Search Results from the CDMS II Experiment*, *Science* **327** (2010) 1619–1621, [arXiv:0912.3592].

[19] **CDMS-II Collaboration** Collaboration, Z. Ahmed *et. al.*, *Results from a Low-Energy Analysis of the CDMS II Germanium Data*, *Phys.Rev.Lett.* **106** (2011) 131302, [arXiv:1011.2482].

[20] G. Gelmini and P. Gondolo, *WIMP annual modulation with opposite phase in Late-Infall halo models*, *Phys.Rev.* **D64** (2001) 023504, [hep-ph/0012315].

[21] R. Schoenrich, J. Binney, and W. Dehnen, *Local Kinematics and the Local Standard of Rest*, *MNRAS* **403** (2010) 1829–1833, arXiv:0912.3693.

[22] J. D. Lewin and P. F. Smith, *Review of mathematics, numerical factors, and corrections for dark matter experiments based on elastic nuclear recoil*, *Astropart. Phys.* **6** (1996) 87–112.

[23] P. J. Fox, G. D. Kribs, and T. M. Tait, *Interpreting Dark Matter Direct Detection Independently of the Local Velocity and Density Distribution*, *Phys.Rev.* **D83** (2011) 034007, [arXiv:1011.1910].

[24] C. Kelso, D. Hooper, and M. R. Buckley, *Toward A Consistent Picture For CRESST, CoGeNT and DAMA*, arXiv:1110.5338.

[25] J. Collar. Talk given at the TAUP 2011 Workshop, Munich, Germany, Sep. 5-9, 2011.

[26] C. McCabe, *DAMA and CoGeNT without astrophysical uncertainties*, *Phys.Rev.* **D84** (2011) 043525, [arXiv:1107.0741].

[27] M. T. Frandsen, F. Kahlhoefer, J. March-Russell, C. McCabe, M. McCullough, *et. al.*, *On the DAMA and CoGeNT Modulations*, *Phys.Rev.* **D84** (2011) 041301, [arXiv:1105.3734].

[28] T. Schwetz and J. Zupan, *Dark Matter attempts for CoGeNT and DAMA*, *JCAP* **1108** (2011) 008, [arXiv:1106.6241].

[29] M. Farina, D. Pappadopulo, A. Strumia, and T. Volansky, *Can CoGeNT and DAMA Modulations Be Due to Dark Matter?*, arXiv:1107.0715.

[30] P. J. Fox, J. Kopp, M. Lisanti, and N. Weiner, *A CoGeNT Modulation Analysis*, arXiv:1107.0717.

[31] M. Vogelsberger, A. Helmi, V. Springel, S. D. White, J. Wang, *et. al.*, *Phase-space structure in the local dark matter distribution and its signature in direct detection experiments*, arXiv:0812.0362.

[32] C. Savage, K. Freese, and P. Gondolo, *Annual Modulation of Dark Matter in the Presence of Streams*, *Phys.Rev.* **D74** (2006) 043531, [astro-ph/0607121].

[33] A. Natarajan, C. Savage, and K. Freese, *Probing dark matter streams with CoGeNT*, *Phys.Rev.* **D84** (2011) 103005, arXiv:1109.0014.

[34] F. Ling, E. Nezri, E. Athanassoula, and R. Teyssier, *Dark Matter Direct Detection Signals inferred from a Cosmological N-body Simulation with Baryons*, *JCAP* **1002** (2010) 012, [arXiv:0909.2028].

[35] J. I. Read, L. Mayer, A. M. Brooks, F. Governato, and G. Lake, *A dark matter disc in three cosmological simulations of Milky Way mass galaxies*, *MNRAS* **397** (2009) 44–51, arXiv:0902.0009.

[36] T. Bruch, J. Read, L. Baudis, and G. Lake, *Detecting the Milky Way's Dark Disk*, *Astrophys.J.* **696** (2009) 920–923, [arXiv:0804.2896].

[37] A. Kurylov and M. Kamionkowski, *Generalized analysis of weakly-interacting massive particle*

searches, *Phys. Rev.* **D69** (2004) 063503, [hep-ph/0307185].

[38] F. Giuliani, *Are direct search experiments sensitive to all spin-independent WIMP candidates?*, *Phys.Rev.Lett.* **95** (2005) 101301, [hep-ph/0504157].

[39] S. Chang, J. Liu, A. Pierce, N. Weiner, and I. Yavin, *CoGeNT Interpretations*, *JCAP* **1008** (2010) 018, [arXiv:1004.0697].

[40] J. L. Feng, J. Kumar, D. Marfatia, and D. Sanford, *Isospin-Violating Dark Matter*, *Phys. Lett.* **B703** (2011) 124–127, [arXiv:1102.4331].

[41] E. Del Nobile, C. Kouvaris, and F. Sannino, *Interfering Composite Asymmetric Dark Matter for DAMA and CoGeNT*, *Phys.Rev.* **D84** (2011) 027301, [arXiv:1105.5431].

[42] M. T. Frandsen, F. Kahlhoefer, S. Sarkar, and K. Schmidt-Hoberg, *Direct detection of dark matter in models with a light Z'*, *JHEP* **1109** (2011) 128, [arXiv:1107.2118].

[43] J. M. Cline and A. R. Frey, *Minimal hidden sector models for CoGeNT/DAMA events*, arXiv:1108.1391.

[44] F. Giuliani, *Isospin conserving Dark Matter with isospin dependent interaction, and reconciliation of contrasting results from direct Dark Matter experiments*, arXiv:1110.4616.

[45] J. Kopp, T. Schwetz, and J. Zupan, *Light Dark Matter in the light of CRESST-II*, arXiv:1110.2721.

[46] S. Chaudhury, P. Bhattacharjee, and R. Cowsik, *Direct detection of WIMPs : Implications of a self- consistent truncated isothermal model of the Milky Way's dark matter halo*, *JCAP* **1009** (2010) 020, [arXiv:1006.5588].

[47] S. Kundu and P. Bhattacharjee, *Neutrinos from WIMP annihilation in the Sun : Implications of a self-consistent model of the Milky Way's dark matter halo*, arXiv:1106.5711.

[48] M. Lisanti, L. E. Strigari, J. G. Wacker, and R. H. Wechsler, *The Dark Matter at the End of the Galaxy*, *Phys.Rev.* **D83** (2011) 023519, [arXiv:1010.4300].

[49] J. F. Navarro, C. S. Frenk, and S. D. White, *The Structure of cold dark matter halos*, *Astrophys.J.* **462** (1996) 563–575, [astro-ph/9508025].

[50] J. D. Vergados, S. H. Hansen, and O. Host, *The impact of going beyond the Maxwell distribution in direct dark matter detection rates*, *Phys. Rev.* **D77** (2008) 023509, [arXiv:0711.4895].

[51] J. Diemand, M. Kuhlen, and P. Madau, *Dark matter substructure and gamma-ray annihilation in the Milky Way halo*, *Astrophys. J.* **657** (2007) 262–270, [astro-ph/0611370].

[52] J. Diemand *et. al.*, *Clumps and streams in the local dark matter distribution*, *Nature* **454** (2008) 735–738, [arXiv:0805.1244].

[53] J. Stadel *et. al.*, *Quantifying the heart of darkness with GHALO - a multi- billion particle simulation of our galactic halo*, *MNRAS* **398** (2009) L21–L25, arXiv:0808.2981.

[54] V. Springel *et. al.*, *The Aquarius Project: the subhalos of galactic halos*, *Mon. Not. Roy. Astron. Soc.* **391** (2008) 1685–1711, [arXiv:0809.0898].

[55] N. Evans, C. Carollo, and P. de Zeeuw, *Triaxial haloes and particle dark matter detection*, *Mon.Not.Roy.Astron.Soc.* **318** (2000) 1131, [astro-ph/0008156].

[56] P. Belli, R. Cerulli, N. Fornengo, and S. Scopel, *Effect of the galactic halo modeling on the DAMA / NaI annual modulation result: an Extended analysis of the data for WIMPs with a purely spin independent coupling*, *Phys.Rev.* **D66** (2002) 043503, [hep-ph/0203242].

[57] N. Evans and J. H. An, *Distribution function of the dark matter*, *Phys.Rev.* **D73** (2006) 023524, [astro-ph/0511687].

[58] L. Hernquist, *An analytical model for spherical galaxies and bulges*, *Astrophys.J.* **356** (1990) 359.

[59] S. Yellin, *Finding an upper limit in the presence of unknown background*, *Phys. Rev.* **D66** (2002) 032005, [physics/0203002].

[60] A. M. Green, *Calculating exclusion limits for weakly interacting massive particle direct detection experiments without background subtraction*, *Phys. Rev.* **D65** (2002) 023520, [astro-ph/0106555].

[61] C. Savage, G. Gelmini, P. Gondolo, and K. Freese, *Compatibility of DAMA/LIBRA dark matter detection with other searches*, *JCAP* **0904** (2009) 010, [arXiv:0808.3607].

[62] **XENON Collaboration** Collaboration, J. Angle *et. al.*, *First Results from the XENON10 Dark Matter Experiment at the Gran Sasso National Laboratory*, *Phys.Rev.Lett.* **100** (2008) 021303, [arXiv:0706.0039].

[63] **XENON10 Collaboration** Collaboration, J. Angle *et. al.*, *A search for light dark matter in XENON10 data*, *Phys.Rev.Lett.* **107** (2011) 051301, [arXiv:1104.3088].

[64] **CDMS Collaboration** Collaboration, Z. Ahmed *et. al.*, *Search for Weakly Interacting Massive Particles with the First Five-Tower Data from the Cryogenic Dark Matter Search at the Soudan Underground Laboratory*, *Phys.Rev.Lett.* **102** (2009) 011301, [arXiv:0802.3530].

[65] K. Schmidt-Hoberg and M. W. Winkler, *Improved Constraints on Inelastic Dark Matter*, *JCAP* **0909** (2009) 010, [arXiv:0907.3940].

[66] **CDMS** Collaboration, D. S. Akerib *et. al.*, *Low-threshold analysis of CDMS shallow-site data*, *Phys. Rev.* **D82** (2010) 122004, [arXiv:1010.4290].

[67] M. Felizardo *et. al.*, *First Results of the Phase II SIMPLE Dark Matter Search*, *Phys. Rev. Lett.* **105** (2010) 211301, [arXiv:1003.2987].

[68] M. Felizardo, T. Girard, T. Morlat, A. Fernandes, F. Giuliani, *et. al.*, *Final Analysis and Results of the Phase II SIMPLE Dark Matter Search*, arXiv:1106.3014.

[69] **CoGeNT** Collaboration, C. E. Aalseth *et. al.*, *Experimental constraints on a dark matter origin for the DAMA annual modulation effect*, *Phys. Rev. Lett.* **101** (2008) 251301, [arXiv:0807.0879].

[70] G. J. Feldman and R. D. Cousins, *Unified approach to the classical statistical analysis of small signals*, *Phys.Rev.* **D57** (1998) 3873–3889, [arXiv:physics/9711021].

[71] A. Brown, S. Henry, H. Kraus, and C. McCabe, *Extending the CRESST-II commissioning run limits to lower masses*, arXiv:1109.2589.

[72] N. Bozorgnia, G. B. Gelmini, and P. Gondolo, *Channeling in direct dark matter detection I: channeling fraction in NaI (Tl) crystals*, *JCAP* **1011** (2010) 019, [arXiv:1006.3110].